Title
HIGH RESOLUTION PHOTOIONIZATION SPECTRUM OF WATER MOLECULES IN A SUPERSONIC BEAM

Author
Page, R.H.

Publication Date
1987-10-01

LBL-24158
Preprint

Lawrence Berkeley Laboratory
UNIVERSITY OF CALIFORNIA

Materials & Chemical Sciences Division

Submitted to Journal of Chemical Physics

High Resolution Photoionization Spectrum of Water Molecules in a Supersonic Beam

R.H. Page, R.J. Larkin, Y.R. Shen, and Y.T. Lee

October 1987

Prepared for the U.S. Department of Energy under Contract DE-AC03-76SF00098

DISCLAIMER

Submitted to Journal of Chemical Physics
PACS 33.80.Eh, 33.80.Gj, 35.20.Vf, 33.70.Fd

HIGH RESOLUTION PHOTOIONIZATION SPECTRUM OF WATER MOLECULES IN A SUPERSONIC BEAM

Ralph H. Page,* Robert J. Larkin,† Y. R. Shen,* and Y. T. Lee†

Material and Chemical Sciences Division
Lawrence Berkeley Laboratory
University of California
Berkeley, California 94720

ABSTRACT

We have obtained high-resolution (~ 1.5 cm^{-1}) photoionization spectra of supersonically-cooled (T_{rot} ~ 50°K) H_2O and D_2O in the 1000-900 A range. The light source, which used the technique of frequency tripling in a pulsed free jet of gas, is described briefly. Spectra are rotationally resolved. Vibrationally-excited autoionizing Rydberg series converging to the ground electronic [$\tilde{X}$; $(1b_1)^{-1}$] state of the molecular ion are detected. This may well be the first example of a highly-resolved Rydberg spectrum of a stable polyatomic molecule. From the convergence limit, the ionization potential of H_2O is determined to be 101777 ± 7 cm^{-1}. Intensities of the Rydberg state autoionization signals are smaller than predicted with known Franck-Condon factors, indicating that predissociation is a competitive decay channel. Rydberg state lifetimes are ~ 1 psec, deduced from homogeneous linewidths.

Autoionizing features from Rydberg states associated with the ion's quasi-linear $\tilde{A}$ $(3a_1)^{-1}$ state are observed with linewidths above 10 cm^{-1}, indicating that their lifetimes are less than ~ 0.5 psec.

Rotational assignments of some of the bands in this linear ← bent transition show that the Rydberg and ionic state geometries are nearly identical. A consistent assignment of the controversial bending (v_2) quantum number and Rydberg series quantum defect $\delta = -0.037$ have been provided.

I. INTRODUCTION

There has been a fair amount of effort spent in analyzing the electronically excited states of the water molecule. At present, there is at least a semiquantitative understanding of some of water's excited states, derived from about 50 years' worth of research. But there is also much that is not known, especially concerning the region above ~ 80000 cm^{-1}, where many excited states exist.

The electronic transitions of water are all in the vacuum ultraviolet (VUV; 2000-1000 A) and extreme ultraviolet (XUV; below 1000 A) regions. A study done by Price[1] detected several absorption bands below the IP (ionization potential) and a pair of Rydberg series converging to it. References to other early works are found in papers by Katayama et al.[2] and Wang et al.[3] As spectroscopic resolution was improved, it became possible to look for rotational fine structure in the electronic transitions. Most of the bands were seen to be rather diffuse, leading to the conclusion that their corresponding excited states were rapidly predissociated. Notable exceptions, in which detailed rotational analyses were performed, were the bands at 1240 A [4] and 1115 A.[5] Vibrational structure built on the intense transitions at 1219 and 1240 A was resolved and analyzed[6] to give values for two of the three vibrational frequencies (ν_1 and ν_2) in the electronically excited states. A simple force-constant model was then used, and is still routinely used, to estimate the value of ν_3, the asymmetric O-H stretch.

There are many transitions of interest near and above the ionization threshold at ~ 980 A, lower in wavelength than the "LiF cutoff" at ~ 1040 A. Windowless XUV (below 1000 A) techniques are

required to study these transitions. In recent years, it has become possible to study resolved absorption features in the XUV region, including Rydberg series converging to the ionization potential. An important work on H_2O and D_2O was done at medium (~ 50 cm^{-1}) resolution by Katayama, Huffman and O'Bryan[2] and gave quantitative absorption and photoionization cross sections between 580 and 1050 A. They discovered some prominent, structured features around 960 A due to autoionizing states, which they studied at higher resolution. The transitions to these states had significant (few cm^{-1}) linewidths and have traditionally been interpreted as a progression in the bending mode ν_2, excited when the molecule snaps from a bent ground state into a quasi-linear excited-state structure. The rotational structure of these autoionizing states has so far not been analyzed, and even the number of bending quanta v_2 in each state is not reliably known.

With a monochromator as the resolution-determining element in laboratory light sources, the trade-off between intensity (signal level) and resolution has prevented the acquisition of well-resolved spectra. The higher-intensity synchrotron light sources have recently been used in obtaining high-resolution (few cm^{-1}) absorption spectra. Studies by Ishiguro et al.,[7] Gurtler et al.,[8] and Connerade et al.[9] have shown detailed fine structure in many bands below the ionization potential. Mayhew[10] has carried out a study of the Rydberg series converging to the IP, with a resolution of better than 1 cm^{-1}. In spite of this, a detailed rotational analysis has not been forthcoming, because the Rydberg region with n (principal quantum number) above ~ 6 is quite congested. There are several overlapping Rydberg series, each of which has vibrational and rotational structure impervious to the use

of high optical resolution. Another problem is that the N_2 molecule has intense absorption lines in this spectral region, and even a slight contamination causes artifacts in absorption spectra.

While Rydberg series below the IP are difficult to study, those above it are not easier: An intense continuum absorption often obscures the weak, discrete lines. To date the autoionizing Rydberg series have not been detected above n ~ 6.

Some information concerning Rydberg series can come from studies of the ionic states to which they converge. In fact, the H_2O^+ ion has been rather well studied. Photoelectron spectra[11-13] have shown the vibrational structure in the $\tilde{X}$, $\tilde{A}$, and $\tilde{B}$ states of the ion. As a result, the ion's geometry in each of these states is roughly known. In the $\tilde{X}$ (ground) state, H_2O^+ has a bent structure much like ground-state H_2O, but it is nearly linear in its $\tilde{A}$ (first excited) state. This fact causes the bending motion to be qualitatively different in the $\tilde{X}$ and $\tilde{A}$ states. In a linear molecule, the vibrational and electronic angular momenta interact. The perturbation, known as the Renner-Teller effect,[14-16] is rather strong in H_2O^+ and has a pronounced effect on the vibronic band structure. The unusual bandshapes which result have long been noted in photoelectron spectra[11-13] and recently displayed with improved resolution by Reutt et al.,[13] who used a supersonic molecular beam of water in their photoelectron spectrometer.

The rotationally resolved H_2O^+ $\tilde{A} \rightarrow \tilde{X}$ spectrum was minutely analyzed by Lew.[17] His determination of the geometries and vibrational frequencies in the $\tilde{X}$ and $\tilde{A}$ states was facilitated by the results from photoelectron spectroscopy, and his much better resolution and subsequent

rotational analysis gave his results considerably greater accuracy.

Studies of the decay mechanisms of electronically-excited water are helping to complete the picture of its behavior. Fluorescence quantum yields have been measured by Lee and Suto.[18] Dutuit et al.[19] have observed wavelength-resolved fluorescence from the predissociation products H ($n \geq 2$) and OH ($\tilde{A}$, $\tilde{B}$). Their fluorescence excitation spectra, obtained over a wide energy range, give detailed information regarding the predissociation characteristics of states associated with individual absorption features. Coupled with the photoionization branching ratio,[2,20] the dissociation and fluorescence quantum yields form a rather thorough catalog of the fates of the molecule in various excited states.

The recent use of the multiphoton ionization (MPI) technique[21-24] has given access to states which do not have electric-dipole transitions from the ground state. When lasers are used, the resolution can be extremely high, so that an accurate rotational analysis is to be expected unless individual rovibronic transitions are so diffuse that they overlap. In fact, the MPI technique has been used to measure homogeneous linewidths of several transitions, with the conclusion that the excited states around 80000 cm^{-1} have rotation-dependent predissociation rates.[22-24] Thus far, multiphoton techniques have not been used to study final states above about 85000 cm^{-1}, but it will be possible to do so when the appropriate lasers are developed.

The effort to deal theoretically with the excited states of water has also been quite extensive. A fairly comprehensive summary of this work is given by Diercksen et al.,[25] who calculated absorption and ionization spectra. They included electric-dipole allowed final-state

orbitals of angular momentum up to 2 (i.e. d orbitals). An "unabashedly empirical" approach was taken by Wang et al.,[3] who attempted to provide a consistent explanation of the known absorption spectra and excited states of water. They did not perform ab initio calculations of energy levels and spectra.

While many features of the water spectrum are basically understood, many details remain to be investigated. Notably, many researchers[3,7,10] do not agree on the assignments and symmetries of the Rydberg series around the IP. Also, the prominent features between the first ($\tilde{X}$) and second ($\tilde{A}$) IP's have not been quantitatively analyzed. A recent work[7] has included a large table of observed transitions, with many unassigned bands. Some means of simplifying the complex spectral region near the IP would clearly be helpful.

We have been able to make some progress in this direction. By using the photoionization technique, we have effectively rejected some absorption features which cause dissociation but not ionization. Autoionization features are then selectively studied. Furthermore, we have used a supersonic expansion to cool the water molecules. The smaller number of ground rotational states populated reduces the number of observed transitions dramatically, and shrinks the "rotational envelope" observed on each electronic transition. As a result, the spectrum becomes much clearer and is more easily interpreted. Finally, we have used the third-harmonic generation (THG) technique to generate the requisite XUV light. This has given us an intense source with good ($\sim$ 1.5 cm^{-1}) resolution, making features with small linewidths retain their prominence in the spectra, and allowing us to determine homogeneous linewidths.

Our technique has given us high-quality spectra of H_2O^+ and D_2O^+ in which we have detected two vibrationally excited autoionizing Rydberg series. From these we derive a new estimate of the ionization potential. Also, we have displayed very intense, well-defined autoionization features which are due to the bending progression in the quasi-linear state. We have done a rotational analysis of some of these bands and determined the vibrational quantum numbers of all of them, allowing us to find the electronic origin of the state. Our analysis contradicts earlier assignments of Ishiguro[7] and Wang[3] and will be useful in testing theoretical calculations of energy levels.

II. EXPERIMENTAL

Figure 1 is a schematic diagram of the components inside our vacuum chamber. Our supersonic sample beam was formed by passing Ne through H_2O or D_2O at 0°C, and admitting the mixture to the beam source region via a Lasertechnics LPV pulsed valve. Its nozzle of 1 mm dia. was ~ 15-20 mm from the 1.25 mm dia. skimmer. With the beam source running at 10 pulses per second, the background pressures in the source and experimental region were ~ 10^{-5} and ~ 10^{-7} torr, respectively; the skimmer provided the only gas leak between the two regions, which had separate pumping facilities. The molecular beam intersected the laser beam between a biased set of ion extraction plates. Photoions were extracted and sent through a differentially pumped (~ 10^{-9} torr) quadrupole mass filter, which was normally run in the high-transmission time-of-flight mode. With all ions created during a nsec laser pulse accelerated to roughly the same kinetic energy, the flight times varied roughly as $\tau \propto \sqrt{M}$. We used a Daly-style ion detector with a Johnston

electron multiplier, and had ion counting capability.

We used a pulsed free jet[26] as the medium for frequency tripling into the 1000-900 Å region. As a windowless system was required, we installed the pulsed free jet source (Newport Research BV-100) in the ion extraction (experimental) chamber. A sleeve/cone arrangement directed the pulse of tripling gas to a separate cryopump, providing differential pumping. Apertures a few mm in diameter in the sleeve transmitted the near UV laser beam to be tripled. The collinear UV and XUV beams intersected the sample beam in the ion extraction region. The experimental chamber pressure rose to only ~ 10^{-6} torr when the tripling gas pulsed valve was running. For best XUV generation, it was necessary to adjust the position of the laser focus in the tripling gas jet. This was done by moving the pulsed valve on an XYZ translation stage, rather than disturb the alignment of the laser and sample beams. We covered the entire 1000-900 Å region continuously by using Ar and Xe as the tripling gases. A more detailed account of our setup, and XUV generation efficiencies obtained with different tripling gases, is published elsewhere.[27]

Our near UV laser source was a conventional system based on a Nd:YAG laser. A Quanta-Ray DCR-1 laser whose output was frequency-doubled pumped a PDL-1 dye laser. We used the dyes Kiton Red 620, Rhodamine 610 Perchlorate, Rhodamine 590, and Fluorescein 548, all obtained from Exciton. The dye laser output was frequency-doubled in an automatically tracked KDP crystal (Quanta-Ray WEX-1). Starting with a 1.06 μ fundamental pulse energy of nominally 700 mj, our tunable near UV pulse energies were on the order of 10 mj. Running the laser at 10 pulses per second and with an easily achieved XUV conversion efficiency

of at least 10^{-7}, the average XUV photon flux would be above 10^{10}/ second. Our XUV bandwidth was ~ 1 1/2 cm^{-1}, making our source much brighter than other laboratory (i.e. discharge) sources. According to Radler and Berkowitz,[28] a discharge lamp/monochromator combination usually gives ~ 10^9 photon/sec in a 30 cm^{-1} bandwidth in this wavelength region. The visible dye laser wavelength was calibrated with an uncertainty of ~ ± 0.5 cm^{-1} by observing the optogalvanic effect[29] in an argon-filled voltage-regulator tube. Our quoted XUV frequencies are thus uncertain to ~ 3 cm^{-1}.

The XUV intensity was quite frequency-dependent, due to resonances in the tripling gas. Also, the various stages of frequency conversion amplified the laser's amplitude jitter and caused a pulse-to-pulse fluctuation of ~ 50% in the number of H_2O^+ ions produced. In order to solve both of these problems, XUV intensity normalization was required. A convenient (but not perfect) normalization technique was to include some C_2H_2 in with the H_2O sample. With two separately delayed gated integrators, we measured the time-resolved H_2O^+ and $C_2H_2^+$ signals separately. For a given ionizing wavelength, the ratio of these two signals was independent of changes, whatever the cause, in the XUV intensity: It depended only on the relative photoionization cross sections of the two molecules. Thus, this ratio can be used with the known C_2H_2 photoionization efficiency curve to find the photoionization efficiency spectrum of H_2O. In the region we studied, the XUV wavelength was less than 990 A, far below the C_2H_2 IP at 1088 A. There is not known to be any intense fine structure in its ionization cross section,[30] but a gradual modulation exists and was imposed on our spectrum. The results we report here concern sharp resonances in the

water molecule and are not noticeably affected.

An extremely advantageous aspect of the use of mass-resolved ion detection was that stray signals from N_2, O_2, and other gases were eliminated. The masses we detected were 18 (H_2O^+), 20 (D_2O^+) and 26 ($C_2H_2^+$) amu. These signals all disappeared when the pulsed valve supplying either the sample or the tripling gas was turned off, proof that they were due only to XUV excitation.

A personal computer controlled the wavelength scans and recorded the averaged $H_2O^+/C_2H_2^+$, H_2O^+, and optogalvanic frequency calibration signals. Depending on the detail we were trying to observe, the dye laser wavelength was incremented by 0.1 A or 0.05 A for each data point, and the averaging time constant was either 3 or 10 seconds. As will be seen in our spectra, the signal-to-noise ratio was quite good.

A crucial parameter was the quality (rotational temperature) of the molecular beam generated in the supersonic expansion, as Fig. 2 shows. In it are two different spectra of the H_2O^+ threshold region. Part (a) is typical of a warm (~ room temperature) sample of gas, as would be produced when the pulsed valve was working poorly or when the sample backing pressure was increased from 200 torr (our normal operating pressure) to 800 torr. In the latter case, the density of gas in the skimmer region may have been great enough to cuase turbulence and loss of rotational cooling. In part (b), a spectrum obtained under normal operating conditions is shown. As will be shown later, the "rotational temperature" of the H_2O molecules was reduced to ~ 50°K, and it is clear that their rotational state distribution has substantially collapsed. It should be noted that all the sharp features in both parts (a) and (b) are real and not noise. Also, in spite of the fact

that the ionization thresholds cannot be rigorously identified, the threshold is seen to appear ~ 200 cm^{-1} higher for the cold molecules, as would be expected: They do not contain as much rotational energy which can contribute to ionization. A closer look at the threshold, obtained with even better signal-to-noise ratio, is provided in Fig. 3. Part (a) is a spectrum of room-temperature gas which was leaked into the chamber, so that its temperature was accurately known to be ~ 300°K. Part (b) is the analogous cold-molecule spectrum.

III. BACKGROUND INFORMATION

In its ground state, water has C_{2v} symmetry, and in order of increasing energy, the electron distribution is described in the molecular orbital picture[31] as $(1a_1)^2(2a_1)^2(1b_2)^2(3a_1)^2(1b_1)^2$. A zeroth-order breakdown into atomic orbitals connects the $1a_1$ and $2a_1$ orbitals with oxygen 1s and 2s electrons. The $1b_2$ and $3a_1$ orbitals come from hydrogen 1s electrons bonded with the oxygen $2p_y$ and $2p_z$ electrons in the molecular plane. Finally, the oxygen $2p_x$ lone pair, sticking out of the molecular plane, is the $1b_1$ orbital, which contributes little to bonding. The overall symmetry of the ground state is $^1A_1$.

The two outermost (highest-energy) orbitals are the ones excited in this experiment. Ionization at threshold corresponds to removal of a $1b_1$ nonbonding electron. This causes the HOH angle to increase ~ 5° and the O-H bonds to lengthen ~ 0.04 Å. Removal of a $3a_1$ H-O-H bonding electron creates the ion's $\tilde{A}$ state, which is quasi-linear.

In the electric dipole approximation, the only forbidden transitions are $a_1 \leftrightarrow a_2$ and $b_1 \leftrightarrow b_2$. Since the molecule is not

spherically symmetric, the orbital angular momentum ℓ is not a strictly "good" quantum number and the atomic $\Delta\ell = \pm 1$ selection rule is relaxed into more of a "propensity rule". Using this rule, we expect transitions of the $p \rightarrow s$ and $p \rightarrow d$ sorts from the $1b_1$ and $3a_1$ orbitals. s states automatically have a_1 symmetry, and there are d states of all four symmetries (a_1, a_2, b_1, b_2). An electron excited to a Rydberg state moves in a nearly central potential, and the orbital angular momentum quantum number ℓ is sensibly employed. For example, the notation $(6da_1, v_1^+ = 1) \leftarrow 1b_1$ describes a transition to the d electron's $n = 6$ state with orbital symmetry a_1, and 1 quantum in the ion core's symmetric stretching (ν_1) vibration. Similarly, the notation $(3a_1)^{-1}$ 3d describes a state in which a $3a_1$ electron has been excited to a 3d state of unspecified symmetry.

When considering rotational transitions, a reference frame is provided by the molecule's principal axes $\hat{a}$, $\hat{b}$, and $\hat{c}$, where $I_a < I_b < I_c$. A rotational state is designated as $J_{K_aK_c}$;[32] in this notation, the total angular momentum J and its projections K_a and K_c on the $\hat{a}$ and $\hat{c}$ axes are given. Since water does not have axial symmetry, K_a and K_c are not rigorously "good" quantum numbers, but the strongest optical transitions can still be listed with selection rules treating K_a and K_c as true angular momentum projections. Different orientations of the transition dipole moment with respect to the molecule's $\hat{a}$, $\hat{b}$, and $\hat{c}$ axes lead to different selection rules for changes in K_a and K_c. In the usual notation, an $\hat{a}$-axis-oriented dipole moment gives "Type A" selection rules and rotational band structure, etc.[31,32]

Spin statistics[31,32] influence the relative rotational line intensities. Fermi statistics apply to H_2O. In its ground (A_1)

electronic state, para-H_2O has even $(K_a'' + K_c'')$ and a statistical weight of 1, [32] and ortho-H_2O, with odd $(K_a'' + K_c'')$, has a weight of 3. D_2O, on the other hand, contains deuterons, which obey Bose statistics. It has weights of 2 in the even $(K_a'' + K_c'')$ states, and 1 in the odd $(K_a'' + K_c'')$ states. In states with B electronic symmetry, the $(K_a + K_c)$ even/odd rule is switched: para (weight 1) states have $(K_a + K_c)$ odd. The $(1b_1)^{-1}$ H_2O^+ ground state (B_1) is an example. The excited states of neutral water can have either A or B electronic symmetry.

IV. RESULTS AND ANALYSIS

Photoionization spectra of H_2O and D_2O in the ~ 100K - 110K cm^{-1} (~ 990-900 A) region are shown in Fig. 4 and Fig. 5, respectively. In each, the baseline represents zero ion signal, so that the cross sections of the sharp features can be reckoned with respect to those of the neighboring continua. As mentioned in the Experimental section, our normalization technique did not give absolute photoionization cross sections. However, reliable continuum cross sections can be gotten from the literature: A photoionization spectrum of room-temperature H_2O, obtained by Eland and Berkowitz[33] with a resolution of 0.14 A (~ 15 cm^{-1}), is shown in Fig. 6. It can in turn be compared with the quantitative spectrum of Katayama et al.,[2] whose resolution was ~ 0.5 A (~ 50 cm^{-1}). They obtained, for both H_2O and D_2O, a photoionization cross section of ~ 6×10^{-18} cm^2 in the plateau just above the IP, with a gradual rise to ~ 8×10^{-18} cm^2 at 900 A. (The baseline has been suppressed in the spectrum of Berkowitz.)

The gross features of Fig. 6 are a threshold at the beginning of a continuum and a number of rather intense structures with ~ 1 A widths

in the 970-910 Å region. These are also visible in Figs. 4 and 5. The most striking difference in our spectra is the presence of a number of intense peaks, which constitute the main subject of this paper. The dips in the D_2O spectrum, marked with a star (*) and appearing at ~ 106350 and ~ 109850 cm^{-1}, are artifacts caused by a gas burst occurring when the liquid nitrogen traps on the diffusion pumps were refilled.

A. Rydberg Series Converging to $\tilde{X}$, $v_1^+ = 1$ of the Ion

(i) Expected Intensities and Missing nd Series

From photoelectron spectroscopy[11] and the thorough visible emission study of the ion[17] it is known that removal of a $1b_1$ (~ $2p_x$ non-bonding) electron causes the ion to "open" and "stretch" slightly with respect to the neutral. The two geometries differ by displacements in the ν_1 and ν_2 normal coordinates. Consequently, if the photon energy is far enough above the IP, the ion can be left in the $v_1^+ = 1$ (symmetric stretching) state, or $v_2^+ = 1$ (bending) state. The photoelectron spectra determine the intensities of these channels to be 0.2 ± 0.04 and 0.1 ± .02, respectively, of the $v_1^+ = v_2^+ = 0$ channel. In the Franck-Condon approximation, the different channels are expected to have qualitatively similar absorption spectra. Just as the vibrationless channel gives a rather sharp ionization threshold followed by a rather uniform direct ionization continuum, the channels with the ion left vibrating should do likewise. Furthermore, the Rydberg converging to the higher ionization thresholds include discrete resonances above the adiabatic IP. Molecules in these states can autoionize and contribute to our spectrum or predissociate into neutral products and go undetected. With simplifying assumptions we sketch how

the spectrum should look above the adiabatic IP if the autoionization yield is 100%. These assumptions are: 1. All observed ionization is due to excitation of the $1b_1$ electron. 2. Within the small energy range we consider, the oscillator strength distribution $df/d\nu$ is constant for each vibrational channel.[33] 3. Only one vibrational channel, the $v_1^+ = 1$ channel, is shown, and only one of the electric-dipole-allowed Rydberg series is shown. Figure 7 is the resulting picture. The heights and frequency spacings of the autoionizing peaks are assumed to have the $1/n^3$ dependence typical of the members of a Rydberg series. The $v_1^+ = 1$ continuum has a Franck-Condon amplitude of 0.2. This intensity would be shared among other Rydberg series converging to the $v_1^+ = 1$ limit, if they were included.

We have detected a pair of Rydberg series in each of the H_2O and D_2O spectra. Transition frequencies for each principal quantum number n are listed in Table I. The lower-frequency transition is listed as "a", the higher-frequency one as "b". We will claim later that the "a" and "b" peaks are different rotational lines in the same vibronic transition. In the H_2O^+ spectrum (Fig. 4), the n = 6 peaks are at 101861 and 101967 cm^{-1}. In the next pair of peaks, n = 7, at 102696 and 102773 cm^{-1}, the relative intensities of the peaks are different: the high-frequency one is weaker. This trend continues as far as the series can be followed, to n = 10 around 103900 cm^{-1}. (The n = 8 peaks are overlapped by other structure.) These series converge at ~ 105000 cm^{-1}.

In the D_2O^+ spectrum (Fig. 5), the first clearly observed members of the series occur at n = 8, at 102525 and 102541 cm^{-1}. These series are well resolved until n = 11, around 103400 cm^{-1}. The n = 12

features are overlapped by a broad structure at 103520 cm^{-1}, and only the low-frequency n = 13 peak is observed, at 103635 cm^{-1}. Extrapolation of these series predicts that n = 7 features should appear at ~ 101990 cm^{-1}. Clearly, there is no lack of resonances in that neighborhood, but a striking resemblance to the $n \geq 8$ bands is not evident. The convergence limits of these series are around 104300 cm^{-1}. In contrast with the H_2O series, in these, the low-frequency member has the greater intensity, presumably because of the differing nuclear spin statistics in the two molecules.

The series do not have the intensity predicted by the model of Fig. 7. Their total intensity should be, according to the known Franck-Condon factor, 20% of that of the continuum. The observed intensity is about ten times less, suggesting that predissociation is an important decay mechanism of Rydberg states.

We identify the observed series with d orbital upper states, in agreement with previous workers. Ishiguro et al.[7] have found peaks at 101864 cm^{-1} and 102712 cm^{-1} in the H_2O spectrum, and assigned them as being part of the $(nd; v_1^+ = 1) \leftarrow 1b_1$ Rydberg series, with n = 6 and 7, respectively. Mayhew[10] has found a peak at 101958 cm^{-1} and similarly assigned it as a $(6d; v_1^+ = 1) \leftarrow 1b_1$ feature. These transition frequencies are near ours but are not coincident. Theoretically, there are many Rydberg transitions from a $1b_1$ orbital; they include s, p, and d final states. But considering that the $1b_1$ orbital is similar to a $2p_x$ lone pair, it is very "atomic" in character. The $\Delta\ell \neq 0$ selection rule would eliminate the np series. Also, comparison of radial matrix elements for hydrogenic wave functions[34] shows that the $2p \rightarrow nd$ series should be much stronger than the $2p \rightarrow ns$ series. In the electric

dipole approximation, four nd Rydberg series of three different symmetries are predicted: nd_{z^2} (a_1), $nd_{x^2-y^2}$ (a_1), nd_{xy} (a_2), and nd_{xz} (b_1). The relative intensities of the four series (in the vibrationless channel) have been calculated by Diercksen et al.,[25] whose prediction is that all four series have nearly equal oscillator strengths; typical strengths for n = 6 are ~ 0.02. Since the Rydberg electron does not significantly influence the motion of the core, there is no reason that the relative absorption intensities of the four series should be significantly different in the $v_1^+ = 1$ state.

In our spectrum, only one series (with associated rotational structure) is apparent. Are the other series rapidly predissociated? Applying the uncertainty principle to the ~ 5 cm^{-1} linewidths of the observed peaks, the total decay (autoionization plus predissociation) rate cannot exceed ~ 10^{12}/sec. A ten times larger predissociation rate of 10^{13}/sec would make a Rydberg series difficult to observe. (This is ~ 10 vibrational periods.) The calculation of autoionization and predissociation rates should probably be done with multichannel quantum defect theory (MQDT).[35] Since this is already challenging for a diatomic molecule, its application to triatomics has apparently not been performed. But we can hypothesize about the missing series in terms of the connection between symmetry and predissociation rate, which is qualitatively understood for the valence excitations.

Even though the words "valence" and "Rydberg" are used to describe excited states, in fact the two are always mixed to some extent. The decay characteristics of the nd ← $1b_1$ Rydberg excitations (a_1, b_1, and a_2) are then partly determined by the valence orbitals they are mixed with. Of the three symmetries, only a_1 has electron density in the

molecular plane, and it should have the greatest propensity for dissociative behavior: $4a_1$ is the lowest unoccupied valence orbital, and is thought to be strongly antibonding.[3,19] This conclusion was reached on the basis of the observed extremely broad absorption features and large dissociation yields. Even higher-lying orbitals with a_1 symmetry would also be slightly anti-bonding. We speculate that rapid predissociation has made the nda_1 series invisible to us. If the a_1 series were not observed, the b_1 and a_2 series would be left for a total of two series. Coincidentally, we have observed two series, but we believe they are really one series with rotational structure. According to our rotational analysis below, the symmetry is a_2.

(ii) Rotational Analysis of H_2O "6a" Feature

The peak we assigned as "6a" in the H_2O^+ spectrum has significant structure, which we observed with high signal-to-noise ratio. Figure 9 shows this region on an expanded scale. Before describing the rotational analysis, we note the presence of the peak which is marked with an arrow (↓) ~ 40 cm^{-1} to the red of the "6b" feature. The reason we do not assign it as "6a" is that its spacing from "6b" is too small to fit the pattern of the other members of the series.

In performing the rotational analysis, we calculated stick spectra by the following procedure. First, partition functions were calculated for H_2O at ~ 30°K and ~ 50°K. In doing this we remained cognizant of the fact that the two spin species (para and ortho) do not interconvert on the timescale of the supersonic expansion. Second, we calculated the fraction of the population in each $J''_{K''_a K''_c}$ state. Third, we calculated the rotational contributions to the rovibronic transition

frequencies. Ground state energy levels came from the tables of Flaud et al.,[36] and approximate n = 6 levels were taken from the ionic-ground-state table of Lew.[17] A diagram of these levels for $J \leq 2$ is shown in Fig. 8. We used the asymmetric rotor rotational line strength tables of Cross, Hainer, and King, as reported by Townes.[32] Stick spectra were constructed for rotational bands of types A, B, and C, at temperatures of ~ 30°K and 50°K. The most intense features in the stick spectra originate from the 0_{00} and 1_{01} states, which are the two lowest in energy, and the only ones populated at extremely low temperatures. The $J'' = 1$ states are at 24, 37, and 42 cm^{-1}, on the order of kT. $J'' = 2$ states begin at ~ 70 cm^{-1} and extend to ~ 135 cm^{-1}. At 50°K, kT ~ 30 cm^{-1}, and only the lowest of the $J'' = 2$ states contribute to the spectrum. Crude calculations of expected spectra can in fact be done by including only the four $J'' = 0,1$ states 0_{00}, 1_{01}, 1_{11}, and 1_{10}. In the D_2O spectrum, and for the same "rotational temperature", more states would need to be included because the spacing between rotational levels is smaller.

Only the "6a" band showed a convincing resemblance to any of the spectra we calculated. The calculated type A ($\Delta K_c = \pm 1$) spectrum of a 50°K sample proved to have intense lines at almost all the right frequencies. Even so, the relative intensities of the lines in the stick spectrum did not agree with those in the experimental spectrum. The source of this problem could be that the branching ratio between predissociation and autoionization depends on the final rotational state. In fact, studies with multiphoton ionization[22-24] have shown that the predissociation rate depends strongly on K_a', the rotation about the â axis. There is not yet a theoretical calculation of this

effect. We have, rather arbitrarily, halved the intensities of the $K_a' = 1$ lines in the stick spectrum in order to improve its fit with the experimental spectrum. Original heights are shown with stars (*).

The â-oriented "Type A" transition causes a $1b_1$ ($2p_x$) electron to be excited into an a_2 state. This excited state cannot be occupied by an s electron, whose wave function must have a_1 symmetry, or a p electron, whose states are of a_1, b_1, and b_2 symmetry. It must contain a d electron. Consequently, we call this the $nda_2 \leftarrow 2pb_1$ molecular analog of the atomic $d_{xy} \leftarrow p_x$ transition induced by a y-oriented (â-axis) electric field. The excitation of the totally-symmetric (a_1) ν_1 vibration during the transition does not change the upper-state symmetry or our symmetry assignment.

Unfortunately, we have not been able to assign, nor did we see, clear rotational structure in any of the other Rydberg features. This is not surprising because the rotational bandshapes look very different in Rydberg states with large n. As the orbiting Rydberg electron is more highly excited, final states of different n become closer together in energy than the rotational level spacing. In this regime a change of basis is appropriate, in which the electronic energy assumes the rôle of a perturbation to the H_2O^+ core rotational energy. Electronic states with different n, ℓ, and orbital symmetry share the same core rotational state $N^+_{K_a^+K_c^+}$. The ordering in energy of the highly-excited Rydberg states is completely different than in the lower states. Line intensities and rotational bandshapes become drastically altered, so that it becomes impossible to identify a band as type A, B, or C.

This phenomenon has been observed in diatomics such as H_2 [37] and Na_2,[38] in which it has been known as "ℓ uncoupling", since the orbital

angular momentum ℓ of the excited electron is no longer locked in space with respect to the ion core. The theory, experimentally confirmed for diatomics, apparently is not well developed for asymmetric rotors like H_2O, which have a nasty rotational energy level structure to begin with. Herzberg has shown that ℓ-uncoupling is nearly complete in H_2 by the time n = 10 for a p electron. In H_2O^+, the rotational constant A ~ 28 cm^{-1} is not very different from the H_2^+ B value of ~ 30 cm^{-1}. This similarity implies that our spectrum, even with its paucity of rotational features, probably includes the effects of ℓ-uncoupling because it includes states with n ~ 10. It would be useful to get data with even better signal-to-noise ratio to analyze with this in mind.

(iii) Convergence Limits and the Ionization Potential

Whenever a Rydberg series is observed, it is possible to find its convergence limit, which is the energy required to form an ion in a given rovibronic state. In both H_2O and D_2O, we have a series rotationally resolved; this situation has not presented itself in previous work on water, nor, to our knowledge, published work on any other polyatomic molecule. Congestion from the large number of thermally populated rotational levels in room-temperature samples has made it impossible to distinguish the a_1, a_2, and b_1 series and find their rotational band origins. In this work, the ion has $v_1^+ = 1$, or one quantum of symmetric-stretching motion. The vibrational frequency ν_1^+ is related to the IP's (all energies in cm^{-1}):

$$IP(v_1^+ = 1) = IP(v_1^+ = 0) + \nu_1^+. \qquad (1)$$

This equation is exact if the rotational state of the ion (i.e. the

rotational energy) is the same in both the $v_1^+ = 0,1$ vibrational states.

In estimating the convergence limits of the "a" and "b" series (Table I), we have made the assumption that all the members within each series ought to be described by the same value of the quantum defect δ in the expression $E(n) = IP - Ry/(n - \delta)^2$. The values of δ and the $n = \infty$ convergence limits are listed in the Table. Our uncertainties in the IP's are due to ambiguities in the choice of the "best fits" and to the calibration uncertainty of ± 3 cm^{-1}. It is seen that the ∞a and ∞b convergence limits are not coincident. This is due to the fact that we have not yet accounted for the rotational energies of the initial state and ion core.

To do a proper job of finding the $v_1^+ = 1$ IP from the Rydberg series would require that we identify the initial rotational states $J''_{K_a''K_c''}$ and final core states $N^+_{K_a^+K_c^+}$ exactly. We are unable to do that because a complete rotational analysis has not been performed, but we <u>can</u> make plausible choices for each of the "a" and "b" series. First, consider the observed intensities: the "a" series is the weaker one in H_2O^+, and the stronger one in D_2O^+. (The "6b" feature in the H_2O^+ spectrum apparently bucks this trend, and thus we exclude the $n = 6$ peaks from the present discussion.) The different nuclear spin statistics in the two molecules are clearly implicated. Thus, H_2O^+ "a" and "b" series are associated with $J''_{K_a''K_c''}$ states of statistical weights 1 and 3, respectively.[31] Conversely, the D_2O^+ "a" and "b" series get the weights 2 and 1. Second, only the initial and final states which cause the strongest autoionization signals need be included. This means that upper states with $K_a' \geq 1$ are rejected on the premise that they are

predissociative. Also, lower states with small populations are ignored.

This leaves (in H_2O) the 0_{00} and 1_{01} initial states, which have the largest populations. After listing the strongest absorption lines from both of them and ensuring that the selection rules for autoionization are obeyed, a limited number of $N^+_{K_a^+K_c^+}$ choices will remain. Since the vibrational autoionization involves the totally- symmetric ν_1 mode, Rydberg and (ion + free electron) states of the same electronic symmetry are coupled. Also, with the ℓ-uncoupled Rydberg electron exerting no torque on the core, no core rotational transitions occur. In this case the autoionization selection rule is simple: no nuclear spin flips (para $\leftrightarrow$ ortho conversions) or changes in core rotational quantum numbers occur.

At energies below the onset of ℓ uncoupling, rotational line intensities can be estimated in the well-understood "coupled" basis, in which the 0_{00} level has equally intense transitions to the upper states 1_{01}, 1_{11}, and 1_{10}. Remembering the nuclear spin statistics, the initial state 0_{00} has para symmetry, as must $N^+_{K_a^+K_c^+}$. Thus, the choices on nuclear spin grounds include the ion states 1_{01} and 1_{10}. Only the first of these has $K_a' = 0$, one of our criteria.

We do not mean to imply that we were actually imposing angular momentum selection rules for the two separate excitation and autoionization processes

$$H_2O + \hbar\omega \rightarrow \ell\text{-uncoupled Rydberg state } H_2O^*$$

$$\ell\text{-uncoupled Rydberg state } H_2O^* \rightarrow H_2O^+ + e^-.$$

More accurately, we made sure, by the use of a simple angular momentum

basis (i.e. ignoring ℓ-uncoupling), that the overall process

$$H_2O\ (J''_{K''_aK''_c}) + h\omega \rightarrow H_2O^+\ (N^+_{K^+_aK^+_c}) + e^-$$

can give a plausible answer for $N^+_{K^+_aK^+_c}$, which determines the series convergence limit. The final states derived by this procedure have the correct symmetries. Use of the inappropriate (ℓ-coupled) basis could only cause an error in the relative intensities of the symmetry-allowed channels.

Based on the criteria above, it is expected that the 0_{00} ground state can produce ions in the 1_{01} state, 21 cm^{-1} above the 0_{00} level. For the 1_{01} ground state, the procedure is the same. In the absence of ℓ-uncoupling, the transition to the 2_{02} level is the strongest. The 2_{02} state also meets the $K'_a = 0$ and nuclear-spin-allowed criteria. This means that the ionic rotational states associated with the "a" and "b" series convergence limits are 1_{01} and 2_{02}, respectively. Note that the $1_{01} \leftarrow 0_{00}$ and $2_{02} \leftarrow 1_{01}$ transitions are both of "Type A", in agreement with our conclusion from the analysis of the "6a" feature. Thus the "a" and "b" series both correspond to $nda_2 \leftarrow 1b_1$.

Since the 1_{01} initial state for the "b" series is 24 cm^{-1} above the 0_{00} ground state, the extrapolated ∞b convergence limit has to be increased by 24 cm^{-1} to give the absolute final energy. Figure 10 is a diagram representing the energy levels involved. With all the rotational levels known, it is possible to predict the difference in observed extrapolated convergence limits (∞b-∞a). This convergence-limit difference should be 17 cm^{-1} for H_2O. Our experimental value of 20 ± 7 cm^{-1} is in good agreement.

This same procedure may be followed for D_2O. All of the rotational constants and energies are roughly half their H_2O values because the deuterium atoms, the major source of the moments of inertia, are twice as massive as hydrogen atoms. The splitting between the ∞a and ∞b convergence limits is thus predicted to be ~ 9 cm^{-1}, in good agreement with our 10 ± 11 cm^{-1} result.

To find the $N^+ = 0$, $v_1^+ = 1$ IP's we subtract 21 cm^{-1}, the rotational energy in the H_2O^+ 1_{01} state, from the H_2O ∞a limit, and 11 cm^{-1} from the D_2O ∞a limit. The results are 104982 ± 5 cm^{-1} for H_2O^+ ($v_1^+ = 1$) and 104289 ± 5 cm^{-1} for D_2O^+ ($v_1^+ = 1$). These values will be used in Eq. (1) to determine the IP of the $v_1^+ = 0$ channel.

Ionization potentials previously determined have ignored the rotational correction, because the rotational lines have never been resolved in the Rydberg or photoelectron spectra. Asbrink and Rabalais[39] did, however, see an asymmetric bandshape in the $v_1^+ = 0$ photoelectron band, obtained with a room temperature sample. In spite of the fact that this band was ~ 400 cm^{-1} wide, they claimed to locate the rotationless origin (the IP) to within ± 8 cm^{-1}. Their assumption was that the rotational transition between neutral and ion must be "type C", because the initial neutral (A_1) and final ion (B_1) states are connected by a $\hat{c}$-oriented (b_1) dipole moment. To find the origin, they superimposed the stick spectrum calculated by Johns[4] for the genuine 1240-Å type C transition on their spectrum. They did not explain why the different angular momentum and symmetry states of the liberated d electron could be ignored; the overall symmetry of the (ion + electron) final state is really a mixture of B_1 multiplied by b_1, a_1, and a_2. This gives not just type C, but type A, B, and C transitions.

There does not appear to be any a priori reason that the "type C" channel has the bulk of the intensity.

Our own estimate of the ($v_1^+ = 0$, $N^+ = 0$) IP comes from subtracting ν_1^+ from the ($v_1^+ = 1$, $N^+ = 0$) IP, as in Eq. (1). Although our experiment did not find ν_1^+, the value obtained by taking the difference of the IP's from photoelectron spectroscopy should be reliable. Reutt et al.[13] have recently recorded photoelectron spectra of molecular beam samples of H_2O and D_2O, with high signal-to-noise ratio and good calibration. Uncertainties in the ν_1^+ frequencies are quite small: ν_1^+ = 3205 ± 4 cm^{-1} for H_2O^+ and 2342 ± 4 cm^{-1} for D_2O^+. Upon subtraction of these frequencies from the ($v_1^+ = 1$, $N^+ = 0$) convergence limits, the rotationless IP's are discovered: 101777 ± 7 cm^{-1} for H_2O and 101947 ± 7 cm^{-1} for D_2O. These values should be better than results of previous experiments, in which the rotational structure was not analyzed in detail. Previous findings, and our new results, are summarized in Table II.

B. Bands Associated with Excitation of a $3a_1$ Electron

(i) Change of Geometry, and Rovibronic Structure

Until now the concern has been the spectral structure due to excitation of an electron in the nonbonding $1b_1$ orbital, the highest occupied orbital. But there are also allowed transitions in the 900-1000 Å range from the next highest filled orbital ($3a_1$), which involves an oxygen $2p_z$ electron. This orbital has appreciable electron density in the plane of the molecule, between the H atoms, and is important in H-O-H bonding. Removal of a $3a_1$ electron causes the ion to have a quasi-linear equilibrium structure, which would also be expected in the $(3a_1)^{-1}$ nℓ Rydberg states. Photoexcitation causes a

sudden transition between the bent (neutral) and linear (ion) geometries, exciting the ν_2 (bending) mode. This is strikingly displayed in the $(3a_1)^{-1}$ band of a photoelectron spectrum; many different v_2^+ states are populated, and the most likely value of v_2^+ is about 8 for H_2O^+ and about 12 for D_2O^+. There is almost zero probability for the $v_2^+ = 0$ state to be created, accounting for the lack of a sharp increase in the ionization yield as the wavelength is decreased to ~ 900 A, the location of the $(3a_1)^{-1}$, $v_2^+ = 0$ IP.

In photoelectron spectra, the vertical transition to the most probable v_2^+ ($n = \infty$) state occurs around 118000 cm^{-1}. Assuming a quantum defect of zero, the n = 3 excitations should be seen $1Ry/(3)^2$ ~ 12000 cm^{-1} lower, at ~ 106000 cm^{-1} in absorption spectra. If autoionization efficiently competes with predissociation, these excitations above the $(1b_1)^{-1}$ IP should also be seen in photoionization spectra. Katayama et al.[2] indeed identified ν_2 progressions in the absorption and ionization spectra. The most obvious examples occur at ~ 104.2K and 106.1K cm^{-1} in the H_2O^+ spectrum (Fig. 4), and ~ 106.6K, 107.3K, and 108.0K cm^{-1} in the D_2O^+ spectrum (Fig. 5). The H_2O^+ peaks occur at ~ 961 and 942 A in the spectrum of Eland and Berkowitz[33] (Fig. 6). There are other peaks seen in their spectrum but not prominently in ours, notably at ~ 952 A (~ 105.0K cm^{-1}), and they all tend to have amplitudes of 10-20% with respect to the continuum ($\equiv$ 100%). Also, they occupy 1-2 A (~ 100-200 cm^{-1}) in the room-temperature spectrum. In our spectra, the sharpest bands are only ~ 50 cm^{-1} wide overall and have about one or two times the intensity of the continuum at their peaks. We attribute this sharpening to a condensation of the rotational structure which occurs when a sample is cooled. Weak

features at 104078 and 105994 cm^{-1} in the H_2O^+ spectrum (Fig. 4), indicated with arrows, appear much stronger when the sample gas is warmer because of poor pulsed valve performance. They must originate from rotational levels which are depopulated by cooling. Higher members of the H_2O ν_2 progression (coincidentally, vertically aligned in the figure), at ~ 108.1K and 110.0K cm^{-1} are quite broad and appear to be rather weak.

None of these ν_2 bands has previously had a thorough rovibronic analysis. Katayama et al. obtained their absorption spectra with a resolution sufficient to find that the individual rotational lines were diffuse, being a few cm^{-1} in breadth. This caused the spectrum to appear congested, hindering rotational assignments. Their list of the strongest absorption lines includes most of the sharp transitions seen in our spectra, with transition frequencies agreeing to within 3 cm^{-1}, our calibration accuracy.

Some features in our H_2O^+ spectrum, for example, at ~ 104.2K cm^{-1} appear to be well-resolved and thus analyzable. Accepting the hypothesis that the three peaks in this band come from a linear ← bent transition, previous rotational analyses of other similar transitions in H_2O^+ [17] and NH_2 [14] can serve as examples for our own assignments, which are described below.

As shown in Fig. 8, in a linear state (like H_2O^+ $\tilde{A}$), the rotational energy levels are given by $BJ(J + 1)$, without regard for K_a and K_c. But for the purpose of describing transitions, it is convenient to retain these projection quantum numbers. Each J state ($J \geq K$) contains both para and ortho nuclear spin modifications, except for $J = 0$, which can have only the 0_{00} level, para in H_2O^+.

Different rotational selection rules are prescribed for treating the vibrational angular momentum due to the linear state's doubly-degenerate bending motion. The origin of the degeneracy is in the $1b_1$ and $3a_1$ ($2p_x$ and $2p_z$) orbitals, which become identical $p\pi_u$ orbitals in the linear configuration. The linear ground state has Σ electronic symmetry, which correlates with the A_1 symmetry of the bent ground state. (The Greek letters identify the axial component of the electronic angular momentum.)

Transitions from the Σ (A_1) lower state to the Π upper state have the transition dipole moment perpendicular to the internuclear axis. The selection rule $\Delta\Lambda = 1$ is obeyed in this case.[31] The corresponding selection rule in the bent-molecule basis is $\Delta K_a = \pm 1$, $\Delta K_c = 0$; this would give rise to a "type C" band.

But when the vibrational angular momentum $\ell = v_2, v_2 - 2, v_2 - 4 \ldots -v_2$ is included, Λ and ℓ are not good quantum numbers because the electronic and vibrational angular momenta interact. The "vibronic" quantum number to use, $K = |\ell \pm \Lambda|$, is analogous to K_a in a bent molecule. The resulting electric dipole selection rule is $K = K_a'' \pm 1$. K is denoted with the capital Greek letters Σ, Π, Δ, Φ, etc. When $\Lambda = 1$, it is seen that even values of v_2 lead to even values of ℓ, odd values of K, and thus Π, Φ, ... states, while odd values of v_2 give Σ, Δ, ... states. Thus the type of vibronic structure observed in the spectrum alternates when v_2 goes from odd to even, etc.

The information just given is sufficient for rotationally analyzing a band due to a single upper (K) state, as will be done here. But for historical completeness it is important to mention that the different <u>vibronic</u> (K) levels within a v_2 band have a strong Renner-Teller

splitting: The degenerate $p\pi_u$ orbitals, mixed by the interaction between vibrational and electronic angular momenta, are strongly nondegenerate in-plane $3a_1$ and out-of-plane $1b_1$ components when the molecule is bent. Then they are ~ 10,000 cm^{-1} different in energy, as manifested in the separation between the IP's $(1b_1)^{-1}$ and $(3a_1)^{-1}$. The different K states are differently perturbed by the vibronic interaction, whose strength is phenomenologically expressed as GK^2, with G ~ - 25 cm^{-1}. According to this relationship, the $\Sigma - \Delta$ (K = 0)/(K = 2) splitting of odd v_2 levels is ~ 100 cm^{-1}, but the $\Pi - \Phi$ splitting of even v_2 states is much larger, at ~ 200 cm^{-1}. When the K structure in a spectrum is not resolved, only the width of a v_2 band can be discerned: the even ($\Pi - \Phi$) bands are "broad", and the odd ($\Sigma - \Delta$) bands are "sharp".

(ii) Rotational Analysis of the Π Bands

Our spectrum is comparatively easy to analyze because only a few transitions are observed, and those are well resolved. In fact, the "broad-sharp" alternation with v_2 has become more of a "band-no band" alternation: bands coming from states with $K_a'' \neq 0$ (i.e. everything but the K = 1 Π bands) are severely weakened by the rotational cooling of the sample.

Our analysis applies to the bands at 104.2K and 106.1K cm^{-1} in the H_2O^+ spectrum (Fig. 4). Figure 11 illustrates the transitions that contribute to these bands and gives the resulting stick spectrum. The final state has Π ($K_a' = 1$) symmetry and the $\Delta K_a = \pm 1$ rule applies, as described above. Initial states can have $K_a'' = 0,2$; the latter are negligibly populated. Thus only two states, 0_{00} and 1_{01}, contribute to the spectrum. The 0_{00} level is the source of an R branch transition to

$J' = 1$, while the 1_{01} level has Q and R branch transitions to $J' = 1$ and 2, respectively. Three peaks are predicted and observed.

The molecule's geometry in the upper state influences the combination difference (peak splitting) R(1) - Q(1). This difference is $4B'$, regardless of whether the upper state is linear, because the 2_{11} (i.e. $J' = 2$) level's rotational energy is $A' + 4B' + C'$, and the 1_{11} ($J' = 1$) level's energy is $A' + C'$. B' varies with the HOH apex angle, being smallest at 180°, when the moment of inertia is largest. Our simulation employed the $(3a_1)^{-1}$ ionic value $B = 9$ cm^{-1},[17] giving a predicted Q-R branch splitting of 36 cm^{-1}. The observed splitting of 37 ± 1 cm^{-1} in both the 104.2K and 106.1K cm^{-1} bands is in good agreement. We can reasonably conclude that the upper states are Rydberg analogs of the quasi-linear $(3a_1)^{-1}$ ionic $\tilde{A}$ state. As discussed in subsection (i), the principal quantum number of the excited electron must be 3.

(iii) ν_2 Numbering and $(3a_1)^{-1}3d$ Energy Level

If the geometry and vibrational level spacings were the same in the $n = 3$ Rydberg state we have observed and in the ion's ($n = \infty$) $\tilde{A}$ state, the ν_2 assignments in the latter would be transferable to our spectra. We did this by plotting the optical (this work) and photoelectron spectra on separate pieces of paper and adjusting the $Ry/(3 - \delta)^2$ relative energy difference for a coincidence. The high resolution photoelectron spectra of Reutt et al.[13] facilitated this process. The various K (Σ, Π, Δ ...) components were not sharply resolved, but were assigned after deconvolution.

Such a "sliding scale" method is not very reliable if only one isotopic species is employed, because the ν_2 levels have rather uniform

spacings and many energy offsets can give peak coincidences. But the $1Ry/(3 - \delta)^2$ electronic energy difference should be the same for H_2O and D_2O. Simultaneous fitting of data on both molecules, whose v_2 spacings are incommensurate, determines the unique solution. Figure 12 illustrates the resulting situation. The separation between the $n = 3$ and $n = \infty$ states should not depend much on differences in vibrational zero-point energies in the molecules, and this test is exceedingly reliable. We have assigned the Σ and Π bands according to their v_2 numbering, both in Tables IIIa and IIIb, and in Figs. 4 and 5. Also, we have computed the difference between each optical transition frequency and the corresponding ion energy level as determined from photoelectron spectroscopy. The result is that $\Delta E \approx 11900$ cm^{-1}, and the quantum defect $\delta \approx - .037$. This value of δ is consistent with that expected for a d electron which has slight overlap with the core. If the similarity in vibrational behavior is maintained even at the lowest v_2 levels ($v_2 = 1$), then the predicted energies of the $3(a_1)^{-1}$ 3d states there are ~ 99740 cm^{-1} for H_2O and ~ 99200 cm^{-1} for D_2O.

Previous authors have differed significantly on the v_2 numbering of the bands, and thus the energy of the $(3a_1)^{-1}$ $n = 3$ origin. Ishiguro et al.[7] proposed a numbering in which all v_2 values were increased by one unit with respect to ours. This caused their $n = 3/n = \infty$ offsets to differ by ~ 200 cm^{-1} between H_2O and D_2O, whereas ours is the same to within ~ 20 cm^{-1} for most bands. Evidently their decision concerning the oddness or evenness of the v_2 bands in the optical spectrum was incorrect; the numbering given for the photoelectron spectrum they employed[12] agrees with ours.[13] Wang et al.[3] proposed a v_2 numbering which differed by 4 units for H_2O and 7 units for D_2O.

The photoelectron data they used[11] erred by one unit in v_2 for D_2O^+. Considering that the levels below $v_2 \sim 4$ have never been observed optically due to the poor Franck-Condon factors and congested spectral regions they occur in, such confusion is understandable.

By knowing the principal quantum number (n = 3) and the quantum defect ($\delta = -.037$) of this v_2 progression, it is possible to predict where transitions to higher Rydberg states should be observed. For example, n = 4 v_2 levels should be 5165 cm^{-1} above their n = 3 counterparts. The n = 4, v_2 = 6 Π band should appear near 109360 cm^{-1} in the H_2O spectrum. There is indeed some structure at that frequency, confirming the prediction. It is a good deal weaker than the n = 3 ← n = 2 transition, as would be expected if it were really due to the n = 4 state.

(iv) $(3a_1)^{-1}$ 3d Oscillator Strength

We estimate the oscillator strength of the n = 3 band which contains the v_2 progression just discussed. Since the continuum cross section is known,[2] it is possible to find the cross section under the peaks and use the relation[33]

$$f = 1.13 \times 10^{12} \int \sigma(\nu) d\nu,$$

where σ is in cm^2 and ν is in cm^{-1}. The cross section of the photoionization continuum is $\sim 10^{-17}$ cm^2; the H_2O peaks are twice as intense as the continuum, rather triangular, and ~ 40 cm^{-1} across. The total oscillator strength of all the peaks in the v_2 progression is a few times 10^{-3}. It is assumed that the autoionization yield is 100%; if not, the oscillator strength has been underestimated by the inverse

of the actual ionization efficiency.

Diercksen et al.[25] calculated oscillator strengths for transitions from $3a_1$ to Rydberg states of all symmetries possible for s, p, and d electrons. They expressed the symmetries in the bent-molecule basis, as is appropriate when a "vertical" transition with no nulcear geometry change occurs. $3d \leftarrow 3a_1$ f values range from 0.004 for the b_1 series to 0.032 for the b_2 series. Our value of a few times 10^{-3} fits the former better. If the b_2 and a_1 symmetries contain states that are highly predissociative, only the b_1 series would occur in the spectrum.

In fact, another series of comparable strength is visible in the H_2O^+ spectrum: its peaks are labeled A, B, C, D, and E (Fig. 4). The "E" peak has a shape similar to a smoothed version of the 3d Π bands of $v_2 = 6,8$. The spacing between v_2 levels is smaller than for the $(3a_1)^{-1}$ 3d progression. This might occur if the excited orbital were slightly antibonding, causing a smaller bending force constant, increased O-H bond length, and larger effective mass for the bending motion. The D_2O^+ spectrum has additional peaks as well, near the n = 3, $v_2 = 13$ Σ, $v_2 = 16$ Π, $v_2 = 15$ Σ, and $v_2 = 17$ Σ bands, as well as at ~ 105350, ~ 107500, and 108310 cm^{-1}. There does not seem to be a pattern in their locations or shapes which is easy to recognize.

(v) Dynamics

In our spectra, the information is in the form of peak heights, widths, and shapes. Peak heights can lead to determinations of branching ratios if total absorption cross sections are known. Also, widths help to determine homogeneous lifetimes. The H_2O highly-resolved $v_2 = 6,8$ Π bands show evidence of states with 0.5 psec lifetimes, as judged from 10 cm^{-1} homogeneous linewidths. Other peaks,

"C" for example, are even broader; it is hard to tell exactly how broad individual lines are because the rotational structure is not resolved. 50 cm^{-1} is a plausible guess, making the lifetime ~ 0.1 psec.

Peak asymmetries are the result of interferences between interacting, optically-accessible channels such as autoionizing (discrete) and ionic (continuum) states. As described by Fano,[40] the fitting of lineshapes gives parameters which are simply interpreted in terms of interaction matrix elements. In a molecule, the dissociation channels must also be considered.

A modest improvement in the signal-to-noise ratio of our H_2O^+ spectrum between 106000 and 106200 cm^{-1} would enable such a lineshape analysis of an isolated, autoionizing resonance. It would help to get the water sample colder so that only two initial states (0_{00} and 1_{01}) are significantly populated. A careful measurement of the photoionization and photodissociation spectra would give the ionization-dissociation branching ratio, the perturbation matrix elements, and the chance to understand a great deal more about the excited states of water.

V. CONCLUSION

We have obtained and partially analyzed photoionization spectra of cold H_2O and D_2O molecules. Our resolution (~ 1 1/2 cm^{-1}) and signal-to-noise ratio were both about ten times better than those in previously reported spectra, enabling us to obtain new information about the all-important water molecule. Autoionizing Rydberg series converging to $v_1^+ = 1$ have been newly observed, and their convergence limits found. By using accurately known values for v_1^+, we have made

improved estimates of the ionization potential. Also, a Rydberg state lifetime (for n ~ 7 - 10) of ~ 1 psec was deduced on the basis of observed linewidths. Several Rydberg series which were expected, did not appear, leading to the conclusion that they are predissociated.

Several rovibronic bands which are part of the $(3a_1)^{-1}$ manifold gave strong autoionization signals and were exposed much more cleanly than ever before, and some were rotationally analyzed. We have compared the energies of the autoionizing states with ionic energy levels determined by photoelectron spectroscopy. From this comparison, we have determined the assignments of v_2 and deduced the adiabatic (v_2 = 1) $(3a_1)^{-1}$ 3d energy level. Lifetimes in some of the v_2 levels appear to be ~ 0.5 psec. This information is useful in formulating theories about the electronic states responsible for the decays.

A really thorough understanding of the highly excited water molecule must be based on accurate data concerning all possible final states. The ionic state is one which is obviously suitable for high-resolution work. Although work has already been done in analyzing the photodissociation spectra,[19] it would be useful to repeat the measurements with a molecular beam sample and higher resolution. This is a much more challenging endeavor than obtaining a photoionization spectrum because fluorescence detection is inherently inefficient with respect to ion detection. But with improvements in the molecular beam source, and large averaging times, it is certainly feasible. Then the missing Rydberg series, supposedly rapidly predissociated, should become visible, even above the IP. With them would come the chance to examine the intramolecular dynamics and their dependences on electronic, vibrational, and rotational state. If this were done it

would probably not be long before multichannel quantum defect theory, currently used on diatomics, was stretched to fit triatomic molecules as well.

VI. ACKNOWLEDGEMENTS

Some electronic data acquisition equipment was borrowed from the San Francisco Laser Center. Dr. Joseph Berkowitz kindly supplied an enlargement of the photoionization efficiency curve of H_2O^+ at room temperature. Dr. Hrvoje Petek made a helpful suggestion concerning the analysis. Dr. Andrew H. Kung provided important advice in setting up the XUV source. This work was supported by the Director, Office of Energy Research, Office of Basic Energy Sciences of the U.S. Department of Energy under Contract No. DE-AC03-76SF00098.

References

1. W. C. Price, J. Chem. Phys. 4, 147 (1936).
2. D. H. Katayama, R. E. Huffman, and C. L. O'Bryan, J. Chem. Phys. 59, 4309 (1973).
3. H.-t. Wang, W. S. Felps, and S. P. McGlynn, J. Chem. Phys. 67, 2614 (1977).
4. J. W. C. Johns, Can. J. Phys. 41, 209 (1963).
5. P. L. Smith, K. Yoshino, H. E. Griesinger, and J. H. Black, Astrophys. J. 250, 166 (1981).
6. S. Bell, J. Mol. Spectrosc. 16, 205 (1965).
7. E. Ishiguro, M. Sasanuma, H. Masuko, Y. Morioka, and M. Nakamura, J. Phys. B 11, 993 (1978).
8. P. Gürtler, V. Saile, and E. E. Koch, Chem. Phys. Lett. 51, 386 (1977).
9. J. P. Connerade, M. A. Baig, S. P. McGlynn, and W. R. S. Garton, J. Phys. B 13, L705 (1980).
10. C. A. Mayhew, Ph.D. Thesis, University of London, 1985.
11. K. Karlsson, L. Mattson, R. Jadrny, R. G. Albridge, S. Pinchas, T. Bergmark, and K. Siegbahn, J. Chem. Phys. 62, 4745 (1975).
12. R. N. Dixon, G. Duxbury, J. W. Rabalias, and L. Asbrink, Mol. Phys. 31, 423 (1976).
13. J. E. Reutt, L. S. Wang, Y. T. Lee, and D. A. Shirely, J. Chem. Phys. 85, 6928 (1986).
14. K. Dressler and D. A. Ramsay, Phil. Trans. Roy. Soc. London, Ser. A 251, 69 (1959).
15. J. A. Pople and H. C. Longuet-Higgins, Mol. Phys. 1, 372 (1958).
16. Ch. Jungen and A. J. Merer, in Molecular Spectroscopy: Modern

Research, K. N. Rao, ed., (Academic Press, New York, 1976), Ch. 3, Vol. 2.

17. H. Lew, Can. J. Phys. 54, 2028 (1976).

18. L. C. Lee and M. Suto, Chem. Phys. 110, 161 (1986).

19. O. Dutuit, A. Tabche-Fouhaile, I. Nenner, H. Frohlich, and P. M. Guyon, J. Chem. Phys. 83, 584 (1985).

20. G. N. Haddad and J. A. R. Samson, J. Chem. Phys. 84, 6623 (1986).

21. M. N. R. Ashfold, J. M. Bayley, and R. N. Dixon, J. Chem. Phys. 79, 4080 (1983).

22. M. N. R. Ashold, J. M. Bayley, and R. N. Dixon, Chem. Phys. 84, 35 (1984).

23. M. N. R. Ashold, J. M. Bayley, and R. N. Dixon, Can. J. Phys. 62, 1806 (1984).

24. G. Meijer, J. J. ter Meulen, P. Andresen, and A. Bath, J. Chem. Phys. 85, 6914 (1986).

25. G. H. F. Diercksen, W. P. Kraemer, T. N. Rescigno, C. F. Bender, B. V. McKoy, S. R. Langhoff, and P. W. Langhoff, J. Chem. Phys. 76, 1043 (1982).

26. C. T. Rettner, E. E. Marinero, R. N. Zare, and A. H. Kung, J. Phys. Chem. 88, 4459 (1984).

27. R. H. Page, R. J. Larkin, A. H. Kung, Y. R. Shen, and Y. T. Lee, Rev. Sci. Inst. 58, 1616 (1987).

28. K. Radler and J. Berkowitz, J. Opt. Soc. Am. 68, 1181 (1978).

29. J. R. Nestor, Appl. Opt. 21, 4154 (1982).

30. T. Hayaishi, S. Iwata, M. Sasanuma, E. Ishiguro, Y. Morioka, Y. Iida, and M. Nakamura, J. Phys. B 15, 79 (1982).

31. G. Herzberg, Molecular Spectra and Molecular Structure. III. Elec-

tronic Spectra of Polyatomic Molecules (Van Nostrand Reinhold, New York, 1966).

32. C. H. Townes and A. L. Schawlow, Microwave Spectroscopy (McGraw-Hill, New York, 1955).

33. J. Berkowitz, Photoabsorption, Photoionization, and Photoelectron Spectroscopy (Academic Press, New York, 1979).

34. E. U. Condon and G. H. Shortley, The Theory of Atomic Spectra (Cambridge Univ. Press, New York, 1959).

35. M. J. Seaton, Rep. Prog. Phys. 46, 167 (1983).

36. J. M. Flaud, C. Cany-Peyret, and J. P. Flaud, Mol. Phys. 32, 499 (1976).

37. G. Herzberg and Ch. Jungen, J. Mol. Spectrosc. 41, 425 (1972).

38. S. Martin, J. Chevaleyre, M. Chr. Bordas, S. Valignat, M. Broyer, B. Cabaud, and A. Hoareau, J. Chem. Phys. 79, 4132 (1983).

39. L. Asbrink and J. W. Rabalais, Chem. Phys. Lett. 12, 182 (1971).

40. U. Fano, Phys. Rev. 124, 1866 (1961).

Table I. Rydberg series converging to H_2O^+, D_2O^+ ($\tilde{X}$, $v_1^+ = 1$).

H_2O			D_2O		
n	$\nu(cm^{-1})$	δ	n	$\nu(cm^{-1})$	δ
6a	101861	0.09	8a	102525	0.14
6b	101967	0.01	8b	102541	0.12
7a	102696	0.10	9a	102903	0.14
7b	102773	0.02	9b	102927	0.09
8a			10a	103171	0.14
8b	103306	0.01	10b	103185	0.12
9a	103616	0.11	11a	103375	0.11
9b	103660	0.03	11b	103405	-.01
10a	103886	0.09	12a		
10b	103926	0.00	12b		
			13a	103635	0.15
			13b		
∞a	105003	± 5	∞a	104300	± 5
∞b	105023	± 5	∞b	104310	± 10

Table II. Ionization potentials from various experiments.

(all values in cm^{-1})

Reference	H_2O		D_2O		Method
	$v_1^+ = 0$	$v_1^+ = 1$	$v_1^+ = 0$	$v_1^+ = 1$	
This work	101777 ± 7	104982 ± 5	101947 ± 7	104289 ± 5	series limit[a]
Karlsson et al.[11]	101746 ± 8	104989 ± 16	101891 ± 8	104255 ± 8	PES[b]
Reutt et al.[13]	101805 ± 30	105010 ± 30	101944 ± 30	104286 ± 30	MBPES[c]
Gurtler et al.[8]	101720		101930		absorption; series limit
Ishiguro et al.[7]	101770		101930		absorption; series limit
Mayhew[10]	101740 ± 10		101910 ± 10		absorption; series limit

[a]extrapolated to ($v_1^+ = 1$, $N^+ = 0$)
[b]photoelectron spectroscopy
[c]molecular beam photoelectron spectroscopy

Table IIIa. Features due to H_2O $3d \leftarrow 3a_1$ transitions, and corresponding ion vibrational levels.

v_2	$\nu(cm^{-1})$	assignment	$\nu^+(cm^{-1})$	$\nu^+ - \nu(cm^{-1})$
4	102330	Π Q(1)		
	102360[a]	Π R(0),R(1)	114237 ± 30	11877
5	103250[a]	Σ	115130	11880
6	104078[b]			
	104172	Π Q(1)		
	104198	Π R(0)	116069	11871
	104209	Π R(1)		
7	105030[a]	Σ	117066	12036
8	105994[b]			
	106081	Π Q(1)		
	106106	Π R(0)	118077	11971
	106118	Π R(1)		
9	107082	Σ	118998	11916
10	108070[c]	Π	119974	11904
11	109080[c]	Σ	120990	11910
12	110020[c]	Π	122033	12013

[a]: uncertain; overlapping structure
[b]: "warm" feature
[c]: broad

Table IIIb. Features due to D_2O $3d \leftarrow 3a_1$ transitions, and corresponding ion vibrational levels.

v_2	$\nu(cm^{-1})$	assignment	$\nu^+(cm^{-1})$	$\nu^+ - \nu(cm^{-1})$
9	104440	Σ	116330	11890
10	105157	Π	117054	11897
11	105862	Σ	117756	11894
12	106582	Π	118487	11905
13	107298	Σ	119196	11898
14	108030	Π	119956	11926
15	108769	Σ	120653	11884
16	109562	Π	121440	11878
17	110267	Σ	122147	11880

Figure Captions

Fig. 1 XUV generation-photoionization apparatus. A supersonic beam of water seeded in neon is delivered via a pulsed valve and skimmer. The beam passes through a set of ion extraction optics. XUV light is generated by frequency tripling in a pulsed jet of xenon or argon. This light ionizes the water molecules in the supersonic beam. Ions are extracted through a mass filter, and counted. Walls which separate differentially-pumped regions are not shown, except for the sleeve and cone which direct the tripling gas into a cryopump.

Fig. 2 Photoionization spectra obtained with different sample temperatures. (a) "Warm" sample obtained by using a high nozzle stagnation pressure. (b) "Cold" sample (normal operating conditions). Rotational temperature is ~ 50°K.

Fig. 3 Photoionization spectra of H_2O^+ near threshold obtained with (a) room temperature gas and (b) the supersonic beam.

Fig. 4 Photoionization spectrum of H_2O^+. Members of "a" and "b" Rydberg series converging to $v_1^+ = 1$ are denoted with their principal quantum numbers. Autoionization features from $(3a_1)^{-1}$ 3d states with ν_2 excited are labeled with their v_2 quantum numbers and the vibronic symmetries of the upper states. Letters A, B, ... identify an unassigned ν_2 progression.

Fig. 5 As in Fig. 4, but for D_2O. Stars (*) indicate artifacts in the spectrum. See text for details.

Fig. 6 Photoionization spectrum of H_2O^+ at room temperature, obtained by Eland and Berkowitz with 0.14 A (~ 15 cm^{-1}) resolution.

The intensity scale is the same in both parts of the spectrum, but the baseline has been suppressed in the second portion. The cross section of the ionization continuum varies from ~ 6 $\times 10^{-18}$ cm^2 near threshold to ~ 8 $\times 10^{-18}$ cm^2 at 900 Å.

Fig. 7 Sketch of the appearance of a single autoionizing Rydberg series, with unit ionization yield. In this case the ratio of the intensity of the autoionizing series converging to the $v_1^+ = 1$ continuum, is just the ratio of the $v_1^+ = 1$ and $v_1^+ = 0$ Franck-Condon factors, assumed to be 0.2 here.

Fig. 8 Rotational energy levels in ground-state H_2O, and the ground and first excited states of H_2O^+. Electronic spin splittings are ignored in the H_2O^+ levels. H_2O levels were taken from Flaud et al.;[34] H_2O^+ $\tilde{X}$ levels are from Lew;[17] and H_2O^+ $\tilde{A}$ energies were calculated with the rotational constant B = 9 cm^{-1}. Nuclear spin labels appropriate for H_2O are shown; the para modification has degeneracy 1, and the ortho modification has degeneracy 3. At 50°K, kT ~ 30 cm^{-1}, and the H_2O $\tilde{X}$ state has most of its population in J = 0,1 levels.

Fig. 9 Detail of n = 6, $v_1 = 1$ H_2O Rydberg state spectrum, and stick spectrum calculated with type A selection rules. Intensities of $K_a' = 1$ sticks have been halved; their original heights are shown with stars (*). The downward arrow (↓) marks an unassigned transition.

Fig. 10 Energy level diagram showing how ∞a and ∞b extrapolated $v_1^+ = 1$ convergence limits are corrected for ground- and excited-state rotational energy offsets. The $v_1^+ = 1$, $N^+ = 0$ IP is thus determined. It can be used to find the $v_1^+ = 0$ IP if ν_1^+ is

known, as from photoelectron spectroscopy.

Fig. 11 (a) Energy level diagram of states contributing to Π upper state in a linear ← bent transition. Realistic ground- and excited-state rotational constants have been used. (b) Resulting stick spectrum. Splittings are in excellent agreement with observations.

Fig. 12 v_2 levels in $(3a_1)^{-1}$ ionic and $(3a_1)^{-1}$ 3d neutral states of H_2O and D_2O. The separation between homologous v_2 levels in the neutral molecule and its ion is independent of isotopic substitution and v_2 level. There is a unique value of $\Delta E = Ry/(3-\delta)^2$ which provides a simultaneous fit to the levels of both isotopomers. ΔE and δ are thus determined. The v_2 numbering in the ion's levels is then transferred to the neutral's, resulting in accurate spectral assignments.

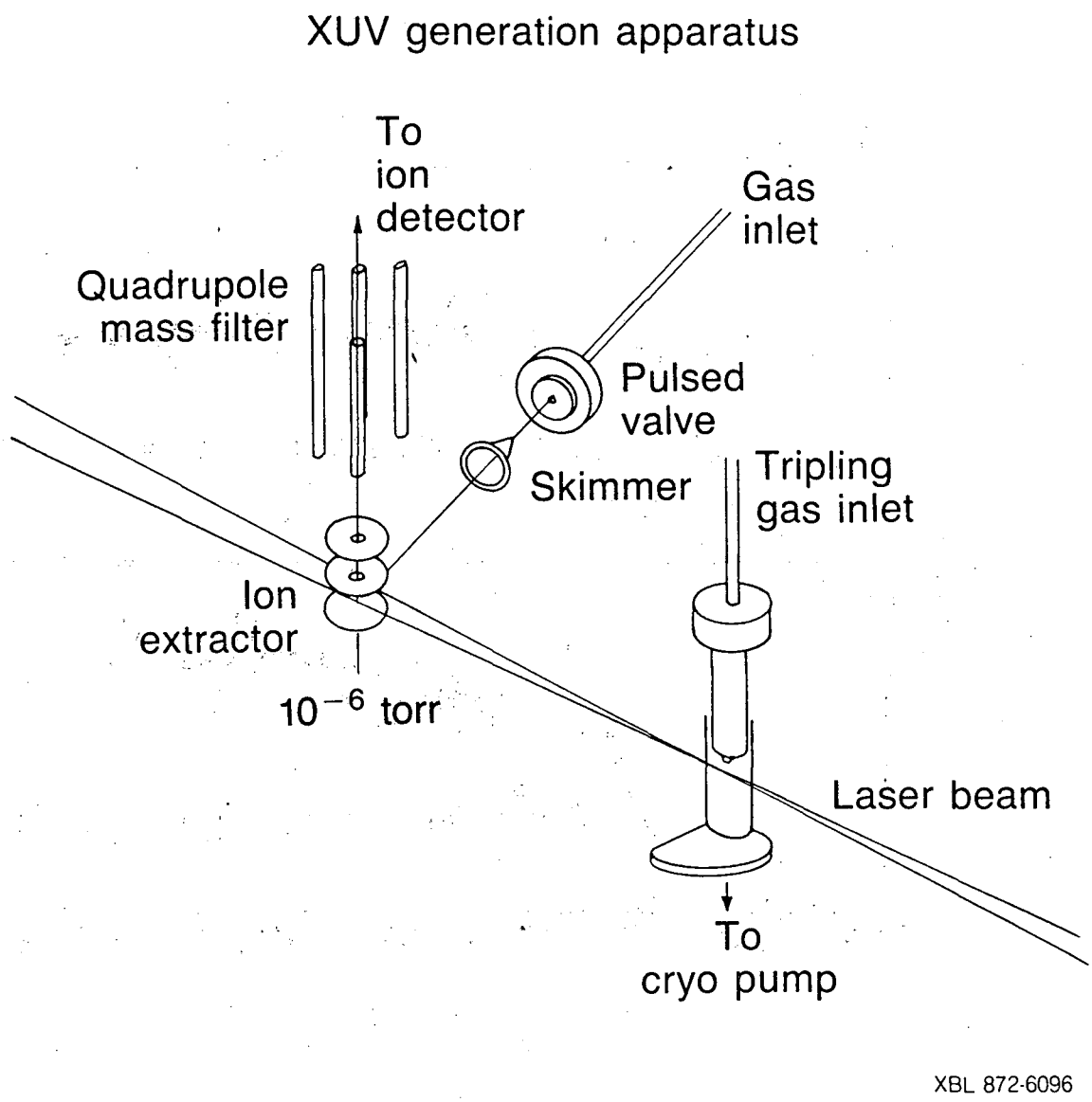
XUV generation apparatus
To
ion
detector
Gas
inlet
Quadrupole
mass filter
Pulsed
valve
Skimmer
Tripling
gas inlet
Ion
extractor
10^{-6} torr
Laser beam
To
cryo pump
XBL 872-6096

Fig. 1

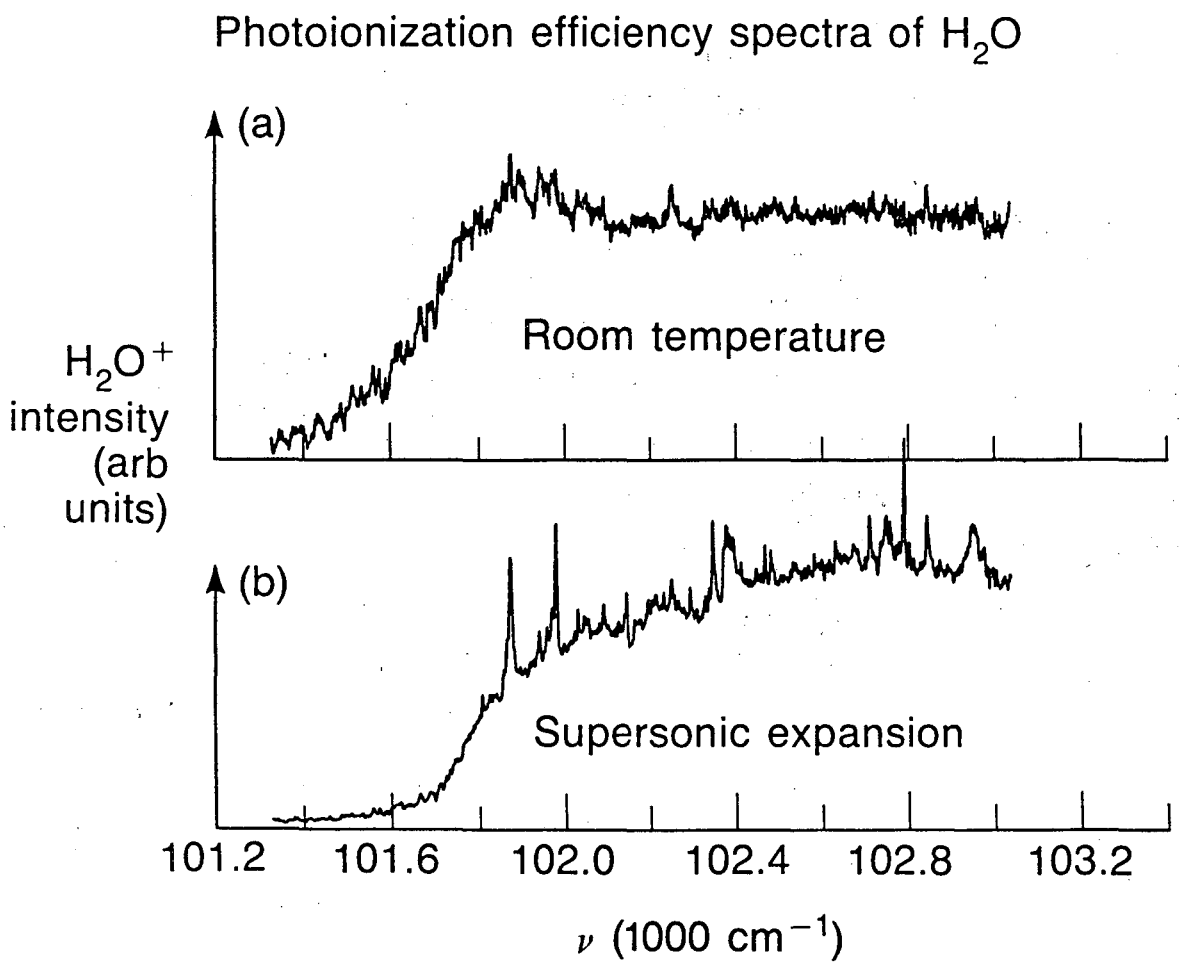
Photoionization efficiency spectra of H_2O
(a)
Room temperature
H_2O^+ intensity (arb units)
(b)
Supersonic expansion
101.2
101.6
102.0
102.4
102.8
103.2
ν (1000 cm^{-1})
XBL 872-6151

Fig. 2

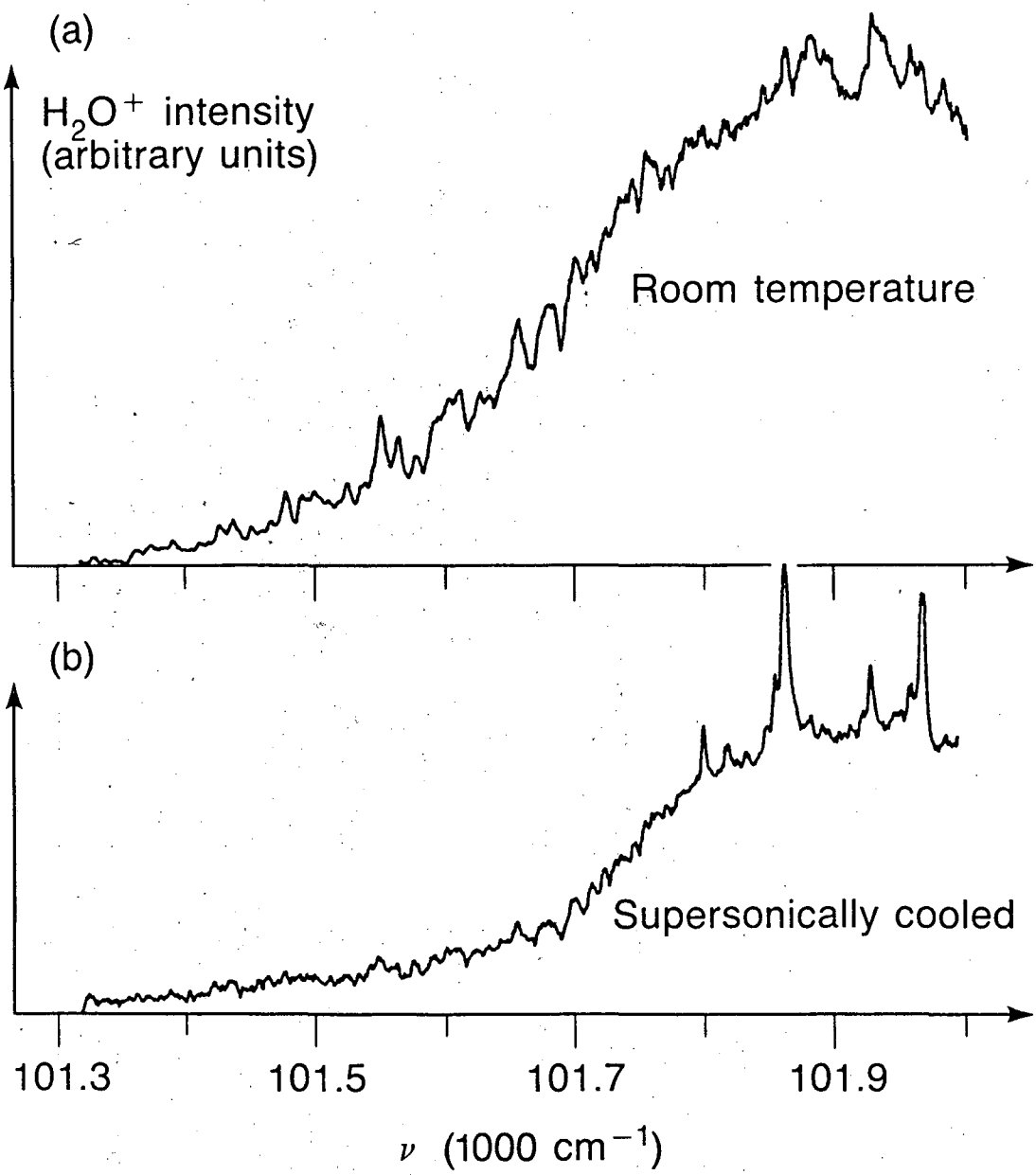
Details of H_2O^+ threshold region
(a)
H_2O^+ intensity
(arbitrary units)
Room temperature
(b)
Supersonically cooled
101.3
101.5
101.7
101.9
ν (1000 cm^{-1})
XBL 872-6127

Fig. 3

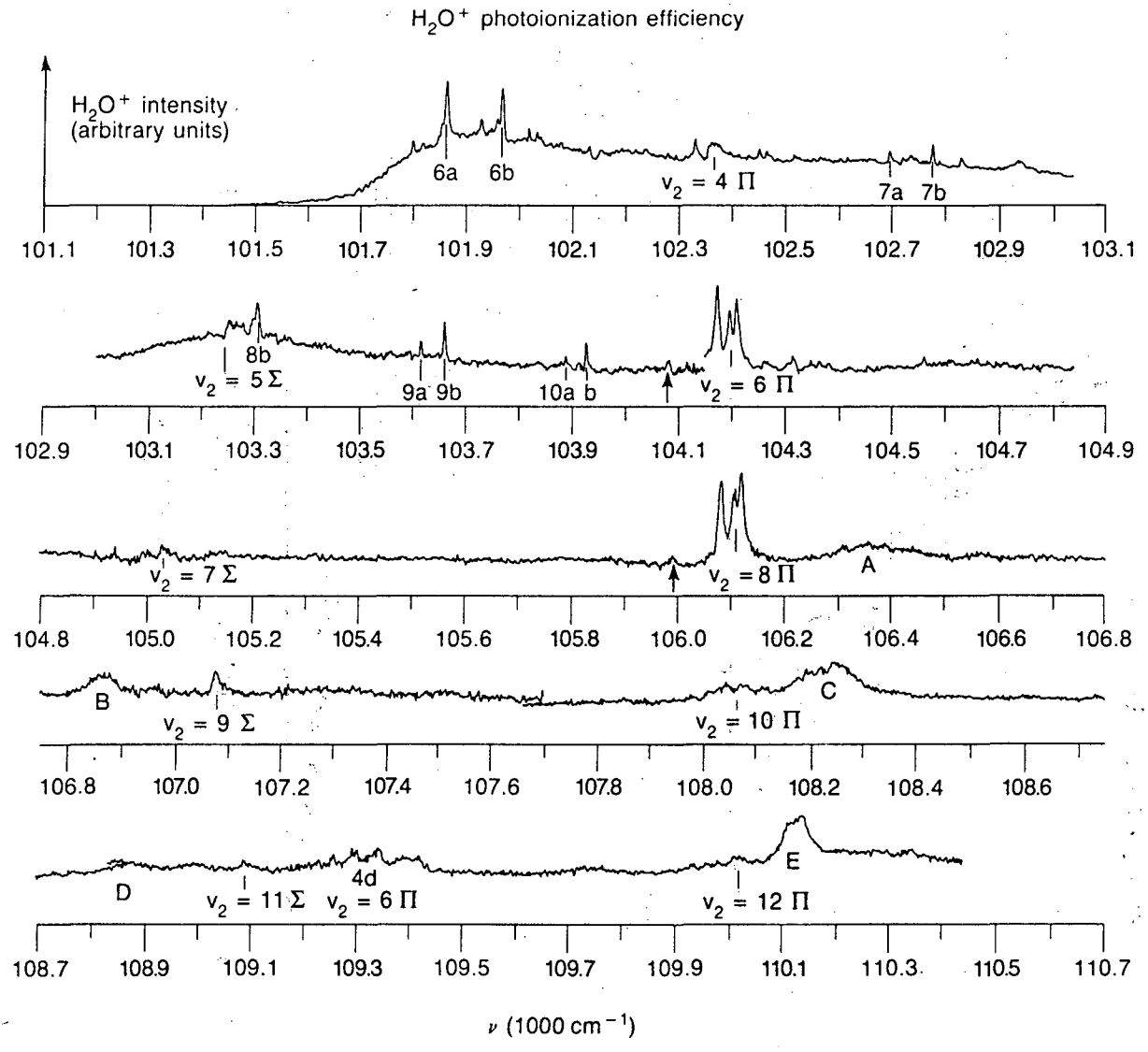
H_2O^+ photoionization efficiency
H_2O^+ intensity (arbitrary units)
6a
6b
v_2 = 4 Π
7a
7b
101.1
101.3
101.5
101.7
101.9
102.1
102.3
102.5
102.7
102.9
103.1
8b
v_2 = 5 Σ
9a
9b
10a
b
v_2 = 6 Π
102.9
103.1
103.3
103.5
103.7
103.9
104.1
104.3
104.5
104.7
104.9
v_2 = 7 Σ
v_2 = 8 Π
A
104.8
105.0
105.2
105.4
105.6
105.8
106.0
106.2
106.4
106.6
106.8
B
v_2 = 9 Σ
C
v_2 = 10 Π
106.8
107.0
107.2
107.4
107.6
107.8
108.0
108.2
108.4
108.6
D
4d
E
v_2 = 11 Σ
v_2 = 6 Π
v_2 = 12 Π
108.7
108.9
109.1
109.3
109.5
109.7
109.9
110.1
110.3
110.5
110.7
ν (1000 cm^{-1})
XBL-872-6148

Fig. 4

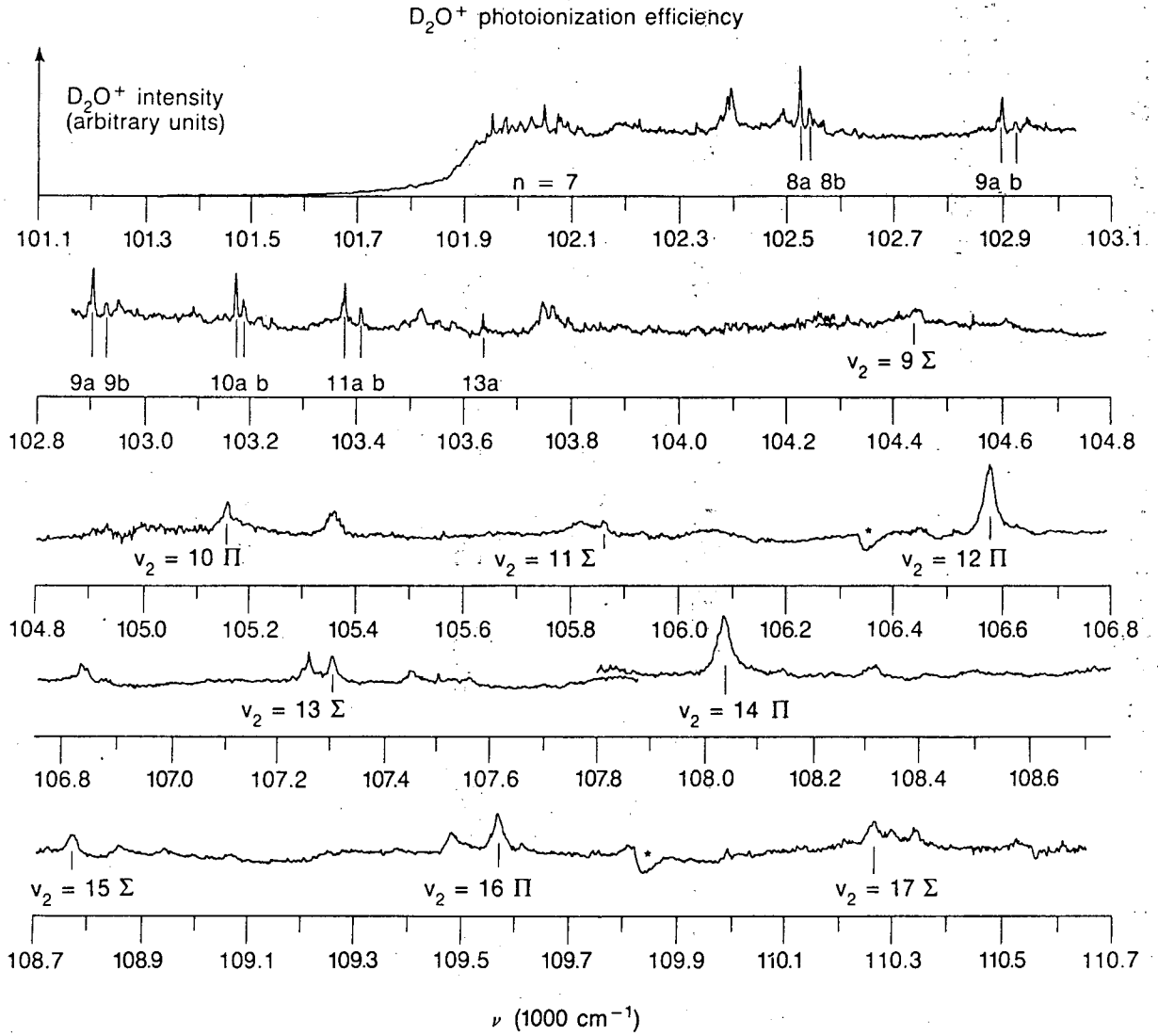

XBL-872-6140

Fig. 5

Photoionization efficiency of room temperature water vapor

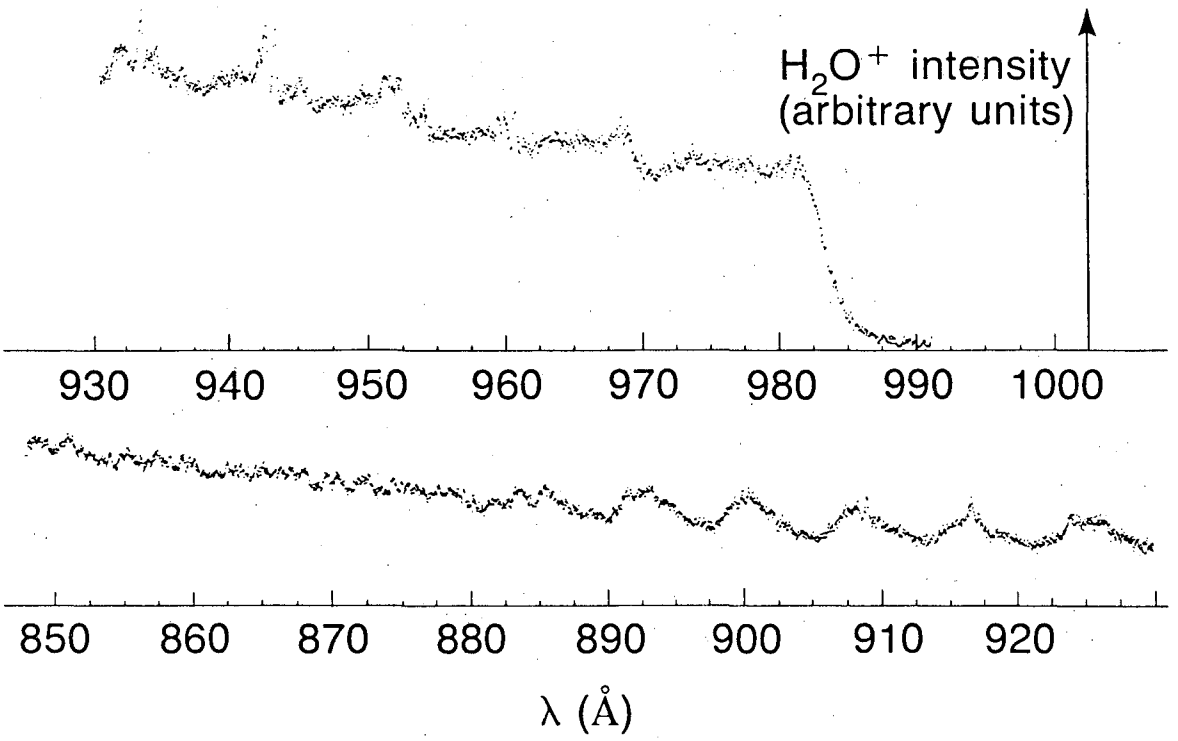

XBL 872-6125

Fig. 6

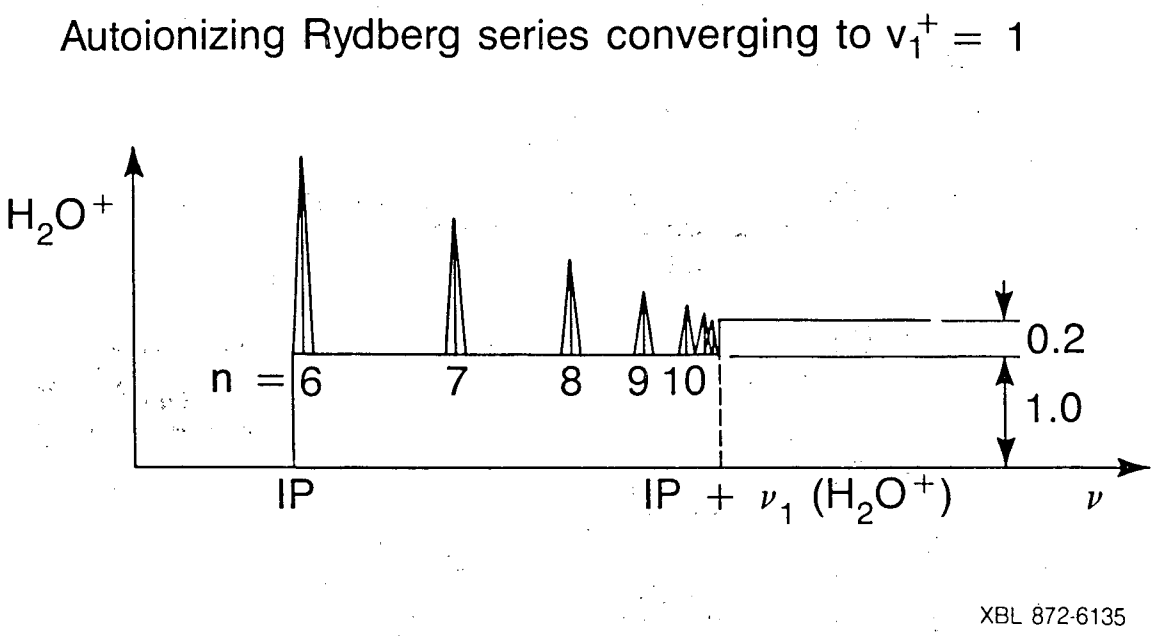
Autoionizing Rydberg series converging to $v_1^+ = 1$
H_2O^+
n = 6
7
8
9 10
0.2
1.0
IP
IP + ν_1 (H_2O^+)
ν
XBL 872-6135

Fig. 7

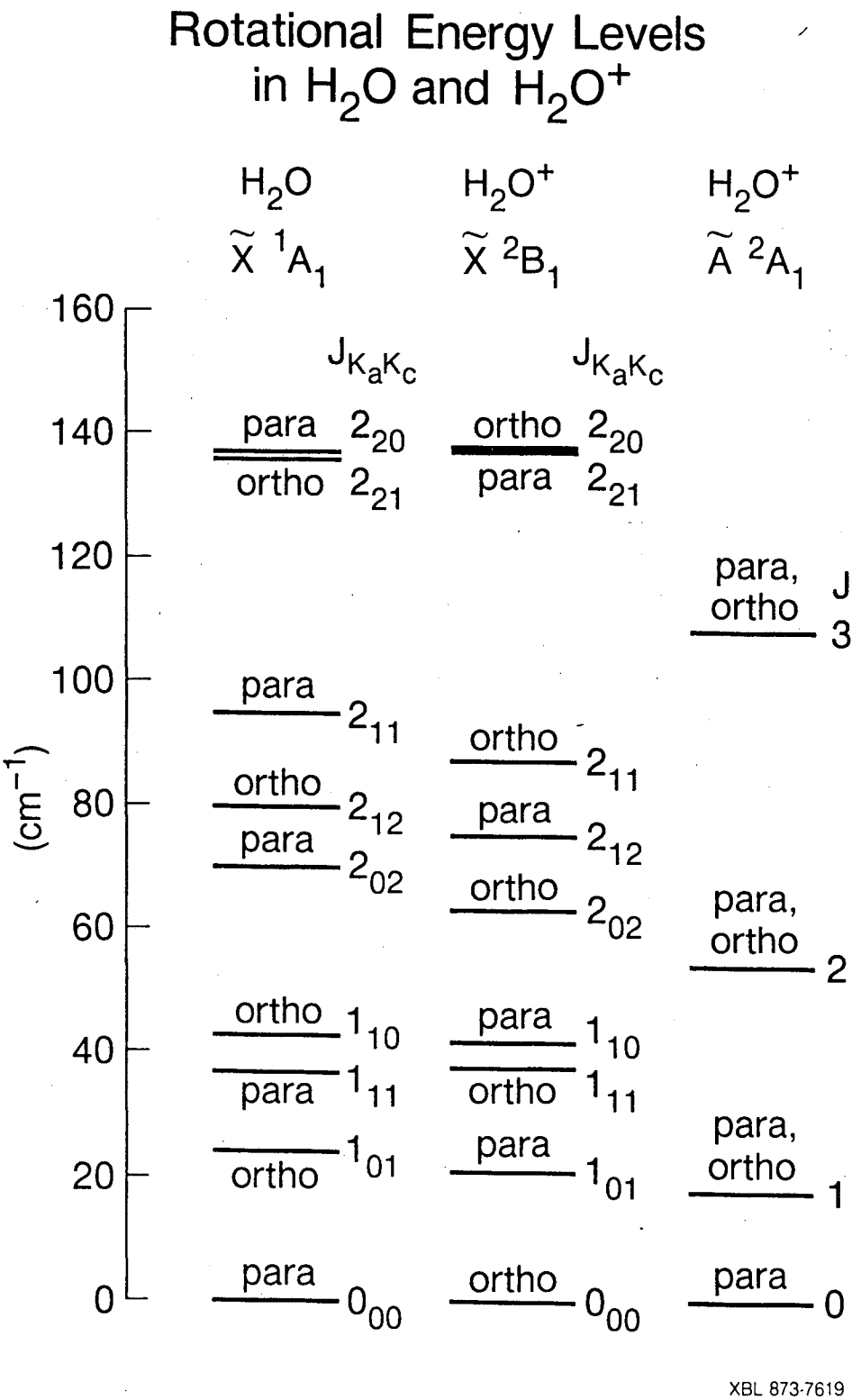
Rotational Energy Levels
in H_2O and H_2O^+
H_2O
$\tilde{X}\ ^1A_1$
H_2O^+
$\tilde{X}\ ^2B_1$
H_2O^+
$\tilde{A}\ ^2A_1$
$J_{K_aK_c}$
$J_{K_aK_c}$
J
(cm^{-1})
160
140
120
100
80
60
40
20
0
para 2_{20}
ortho 2_{21}
ortho 2_{20}
para 2_{21}
para, ortho 3
para 2_{11}
ortho 2_{12}
para 2_{02}
ortho 2_{11}
para 2_{12}
ortho 2_{02}
para, ortho 2
ortho 1_{10}
para 1_{11}
1_{01} ortho
para 1_{10}
ortho 1_{11}
para 1_{01}
para, ortho 1
para 0_{00}
ortho 0_{00}
para 0
XBL 873-7619

Fig. 8

Comparison of Experimental Spectrum With Stick Spectrum of a Type A Band

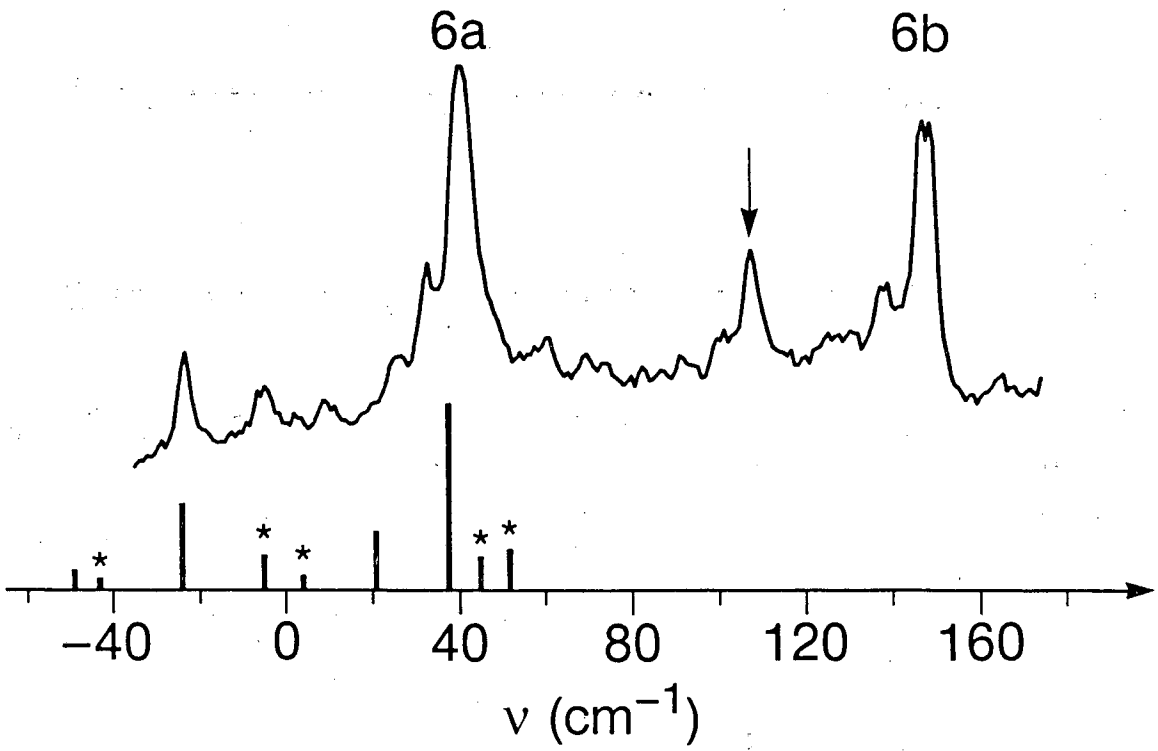

XBL 873-7623

Fig. 9

Determination of Rotationless ($N^+ = 0$) Convergence Limits of $v_1^+ = 1$ "a" and "b" Series

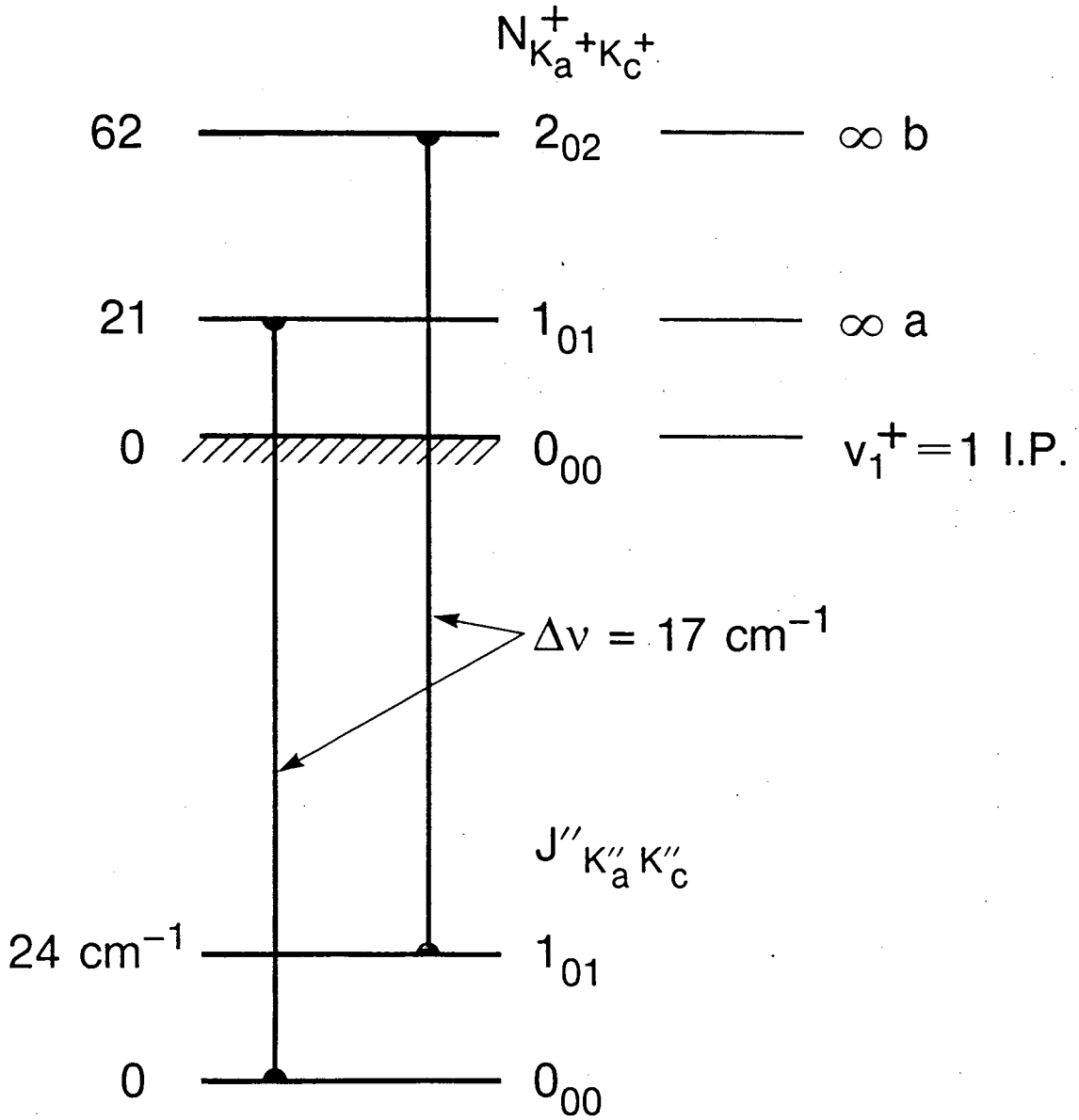

Fig. 10

XBL 873-7621

Rotational Structure of Π Bands in a Linear ← Bent Transition

(a)

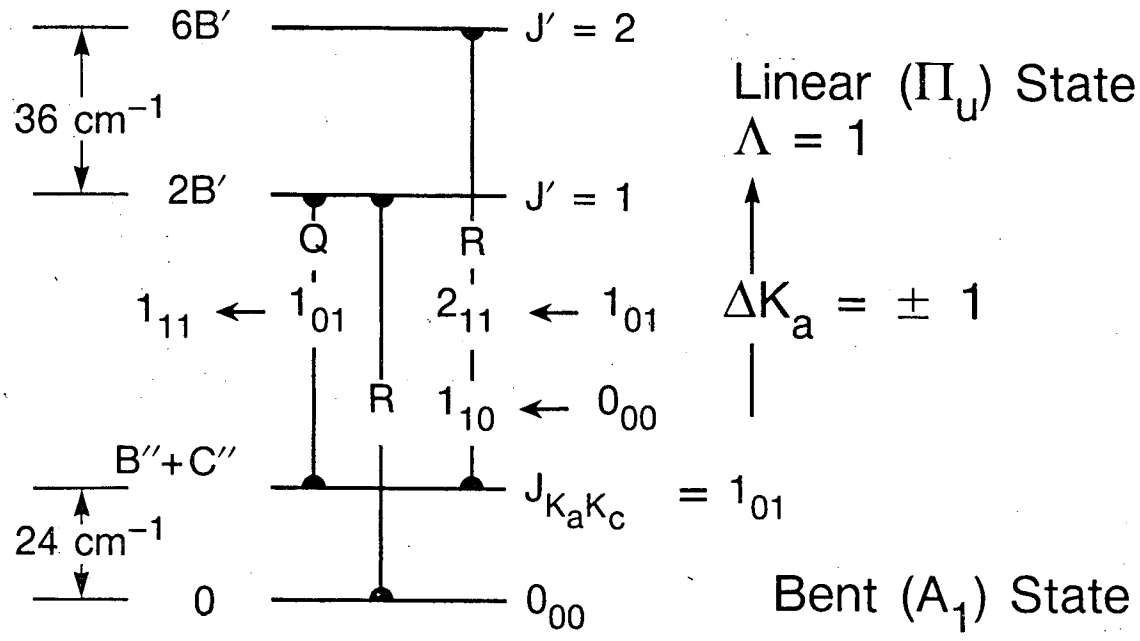

(b)

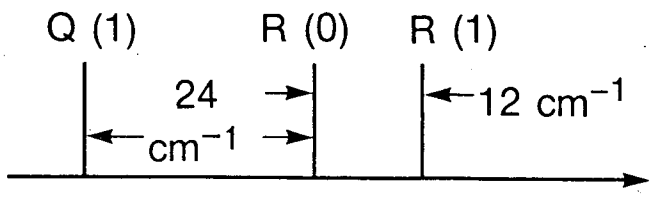

XBL 873-7618

Fig. 11

Assignment of V_2 Levels and $(3a_1)^{-1}$ 3d Energy

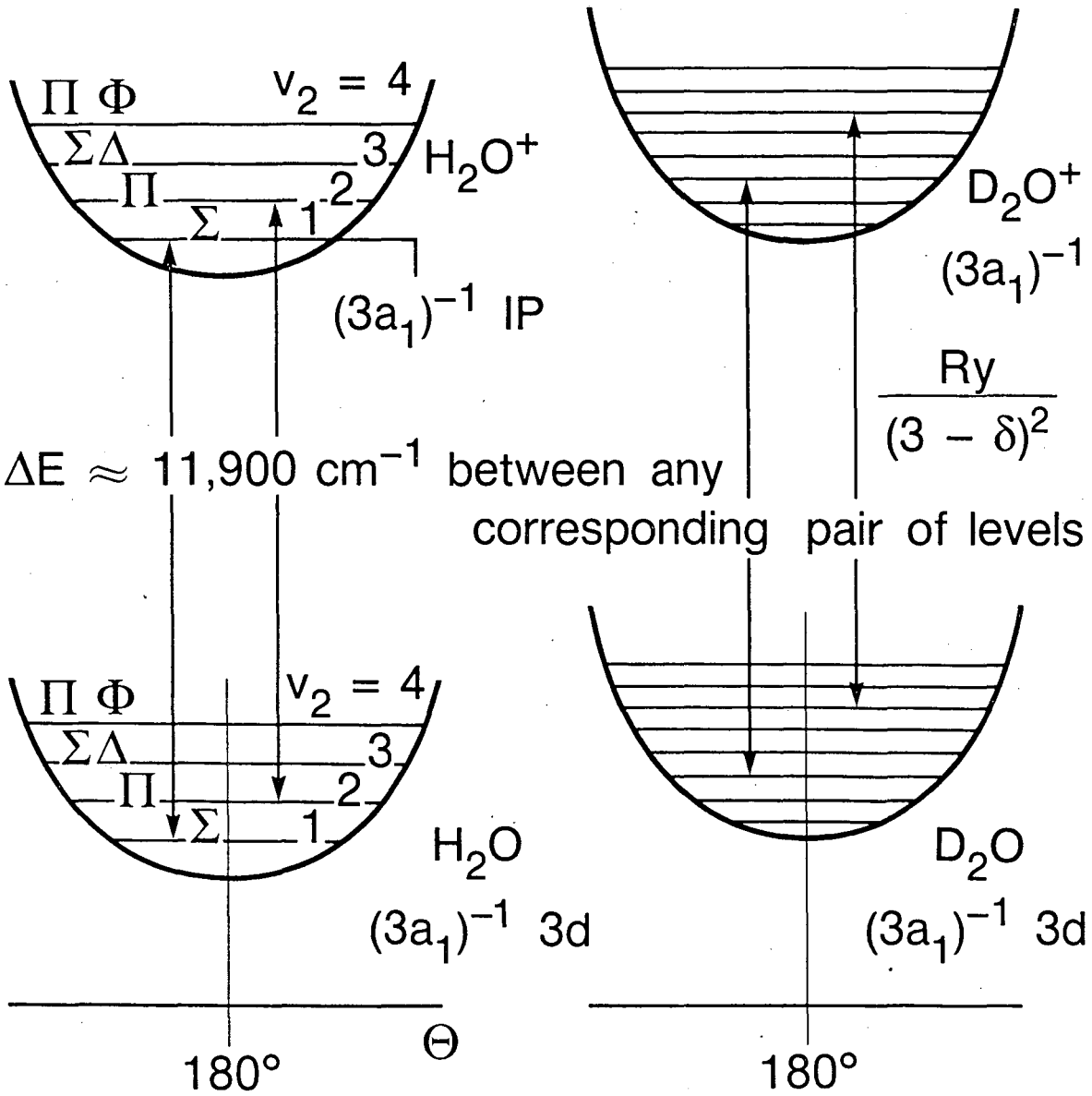

XBL 873-7622

Fig. 12

LAWRENCE BERKELEY LABORATORY
TECHNICAL INFORMATION DEPARTMENT
UNIVERSITY OF CALIFORNIA
BERKELEY, CALIFORNIA 94720